

Recent Progress in Transistor-Based Optoelectronic Synapses: From Neuromorphic Computing to Artificial Sensory System

Sung Woon Cho, Sung Min Kwon, Yong-Hoon Kim,* and Sung Kyu Park*

Neuromorphic electronics draw attention as innovative approaches that facilitate hardware implementation of next-generation artificial intelligent system including neuromorphic in-memory computing, artificial sensory perception, and humanoid robotics. Among the various neuromorphic devices, optoelectronic synapses are promising neuromorphic devices that use optical means to mimic synaptic plasticity and related functions. Compared with classical neuromorphic chip based on electronic synapses using electrical means, photonic neuromorphic chip using light as input spike signal can be attractive alternative approach for next-generation artificial intelligent system capable of high density, low power consumption, and low crosstalk. Thus, various optoelectronic synaptic electronics have been developed to overcome the drawback of conventional artificial intelligent system based on electrical synapses. Herein, the recent progresses in transistor-based optoelectronic synapses for artificial intelligent system and review their device architecture, neuromorphic operational mechanisms, manufacturing methodologies, and advanced applications for artificial intelligent computing and visual perception systems are focused. Finally, the future challenges and research direction in the optoelectronic synaptic research are discussed.

can simultaneously perform the calculation and memory of massive information received from peripheral nervous system (PNS).^[4] It is believed that synaptic plasticity and its event-driven updating functions by repetitive stimuli of spike-form are key factors of power-efficient computing.^[5] Therefore, neuromorphic electronics that can mimic key element for in-memory computing performance of biological CNS have been developed, as a neuromorphic computing device (artificial brain) of hardware-type artificial intelligence computing systems.^[6–8] Compared with traditional digital-logic von Neumann-based computing, CNS-inspired neuromorphic electronic-based computing is advantageous for power-efficient and space-saving processing of massive information data. Meanwhile, the PNS consists of sensory and motor nerves.^[3] The CNS and PNS work together to recognize external information, make appropriate decisions, and control the mechanics of the body. Humans can recognize information from


1. Introduction

Neuromorphic electronics, which can mimic the key functions of the human nervous system, are attracting attention as an innovative approach that facilitates the hardware implementation of next-generation artificial intelligence systems, such as neuromorphic in-memory computing, artificial sensory perception, and humanoid robotics.^[1–3] The central nervous system (CNS, e.g., the brain and the spinal cord) is biological computer which

external stimuli (e.g., light, pressure, sound, gas, and flavor) through a biological sensory system consisting of the sensory part of the PNS and the computational part of the CNS. The sensory part of the PNS (sensory organs and nerves) detects external stimuli (e.g., light, pressure, sound, gas, and flavor), and the computing part of the CNS recognizes stimuli information and makes appropriate decisions. Therefore, the artificial sensory perception system can be realized by developing neuromorphic electronics which integrate neuromorphic computing device and

Prof. S. W. Cho
Department of Printed Electronics Engineering
Suncheon National University
Suncheon, Jeonnam 57922, Republic of Korea

S. M. Kwon, Prof. S. K. Park
School of Electrical and Electronics Engineering
Chung-Ang University
Seoul 06974, Republic of Korea
E-mail: skpark@cau.ac.kr

 The ORCID identification number(s) for the author(s) of this article can be found under <https://doi.org/10.1002/aisy.202000162>.

Prof. Y.-H. Kim
School of Advanced Materials Science and Engineering
Sungkyunkwan University
Suwon 16419, Republic of Korea
E-mail: yhkim76@skku.edu

© 2021 The Authors. Advanced Intelligent Systems published by Wiley-VCH GmbH. This is an open access article under the terms of the Creative Commons Attribution License, which permits use, distribution and reproduction in any medium, provided the original work is properly cited.

Prof. Y.-H. Kim
SKKU Advanced Institute of Nanotechnology (SAINT)
Sungkyunkwan University
Suwon 16419, Republic of Korea

DOI: 10.1002/aisy.202000162

functional sensors such as optical, chemical, and haptic sensors.^[9–12] In addition, humans use the motor part of the PNS (motor nerves and organs) to represent outputs that correspond to decision-making outcomes in sensory perception system. Therefore, the development of advanced neuromorphic electronics incorporating neuromorphic computing devices, functional sensors, and additional actuators (artificial motor organs) is steadily progressing for the realization of humanoid robots with human-like perception and motor functions.^[13–16]

Among neuromorphic electronics, optoelectronic synapse is representative component which can emulate synaptic plasticity behavior and related functions in optical manner, which enables to implement photo-neuromorphic computing and artificial visual perception system.^[17,18] Compared with classical neuromorphic chip based on electronic synapses using electrical manner, it is expected that photoneuromorphic chip using optoelectronic synapses will be more beneficial for high-speed and high-density processing of massive information due to low power consumption and low mutual interference of optical input signals.^[19,20] Using the well-designed optical waveguides that enable total reflection, mutual interference between different optical inputs can be minimized during transmission.^[21,22] In contrast, in the case of the electric synapses, it is relatively difficult to suppress mutual inference caused by an electromagnetic field generated from an electric bias signals transmitted along electric wires. In addition, the excellent optical response of optoelectronic synapses allows the integration of artificial vision perception system capable of simultaneously collecting and computing external visual information.^[23] There are different types of devices designed to manufacture optoelectronic synapses: memristor, thin-film transistor (TFT), and phase change memory.^[24–28] The memristor-type optoelectronic synapses are suitable for high-density integration and large-area scalability using cross-bar arrays.^[29–31] Nevertheless, system-level issues such as low uniformity, cyclic operational instability, and sneak-current phenomena should be addressed. In contrast, despite relatively complex device structure, the transistor-type optoelectronic synapses are advantageous for linear conductance

switching, high uniformity, long-term operation durability, and artificial sensory platform due to difference of driving mechanism.^[32–34] In the case of transistor-type optoelectronic synapses, optically triggered photosynaptic plasticity can be investigated by monitoring light-induced analogue switching and event-dependent retention duration of channel conductance between in-plane directional two electrodes (source and drain). Meanwhile, the gate-terminal of transistor-type optoelectronic synapse serve as an electrical modulator of photosynaptic output signals or transmission path of inhibitory electrical inputs.^[35,36]

In this Review, we focus on the recent advances in transistor-based optoelectronic synapses and their advanced applications for artificial intelligent computing and vision perception systems (Figure 1). In Section 2, we discuss basic knowledge about biological synapses and essential synaptic functions which should be mimicked by artificial synapses. In Section 3, transistor-based optoelectronic synapses with photosynaptic plasticity and related functions are discussed in terms of the device architectures and device physics. In Section 4, we explore advanced functions demonstrated at optoelectronic synapses for photoneuromorphic computing. In Section 5, we review the artificial photosensory system implemented using optoelectronic synapses and their advanced functions. In the end, we give future research directions of optoelectronic synapses toward artificial intelligent systems including computing, sensory perception, and smart robotics.

2. Biological and Artificial Synapses

2.1. Function and Structure of Biological Synapse

Learning is an important biological computing behavior that underlies cognitive function. It can induce continuous behavioral changes based on memories that arise from continuous experiences. So far, the complete biological mechanism for learning has not been established. However, it is estimated that the connection changes of the neural network of the brain by learning of knowledge are stored in the form of weight of synapses between

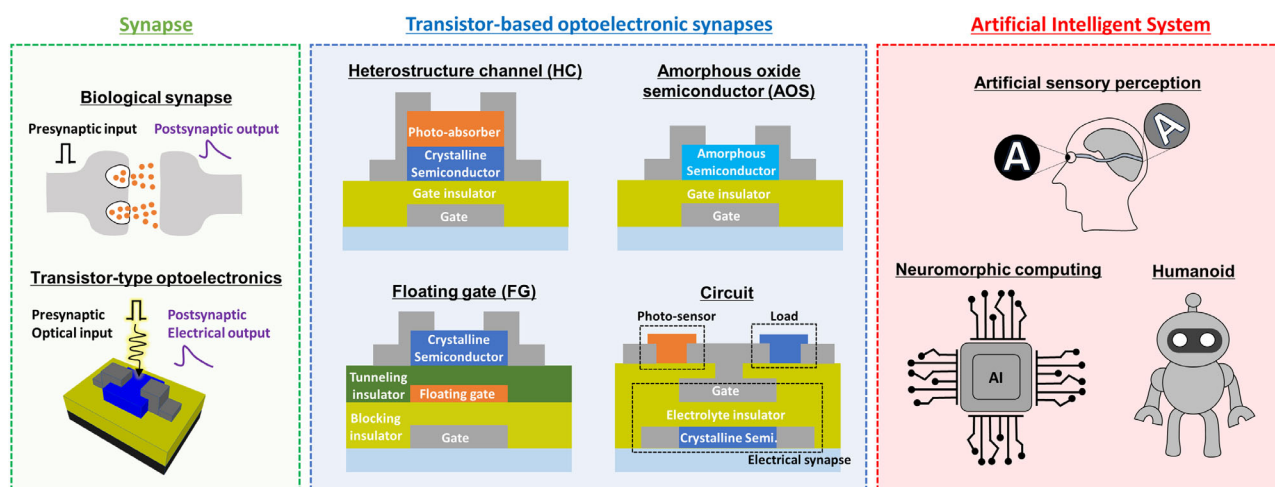


Figure 1. The transistor-based optoelectronic synapses with photosynaptic plasticity and related neuromorphic functions and their advanced application for artificial intelligent system including neuromorphic in-memory computing chip, artificial sensory perception, and humanoid robotics.

neurons. Neuroplasticity is a phenomenon in which neuropaths are structurally and functionally changed and reorganized by external stimuli and experiences. Based on the plasticity of the neural network, living things have the property of adapting to specific external environmental factors, and the brain can learn tailored to the environment and individual behaviors. In the brain, neuron is a basic building blocks of nerve cells composed of dendrites, nerve cell body, and axons (Figure 2a).^[37,38] Neuron generates action potentials in the excited or restrained states and transmits signal information to the next neuron. In nerve fibers, there is a difference in ion concentration inside and outside the cell membrane, so a potential difference occurs (Figure 2b).^[39,40] The action potential instantaneously changes the ion concentration around the cell membrane, and again generates a potential signal continuously to transmit a voltage potential signal. The signal transmitted to the presynaptic axon terminal is then released by leaking the neurotransmitter to the lower membrane of the synapse and then to the receptor of the next neuron. This voltage signal arrived at the presynaptic axon terminal is then delivered by leaking the neurotransmitter to the postsynaptic membrane and dendrite of next neuron (Figure 2c), indicating the synapse connection.^[39,40] When these synaptic connections are accumulated, signal transmission potentiates/depresses, resulting in long-term strengthening/weakening. Long-term

plasticity is considered as a symbol of learning from simple classical conditioning to complex higher order thinking. In this regards, recent research trends for neuromorphic electronics are attempting to emulate the biological synaptic behavior using single optoelectronic devices or the neural network using system-level device arrays.

2.2. Emulation of Synaptic Functions using Artificial Synapse

In the artificial neural network systems, neuromorphic electronics have been demonstrated as simplified neurons, and there are attempts to implement the neural networks through system-level on-chip integration of the neuromorphic devices.^[1,2] To understand the activity of numerous neurons that are complexly linked, it becomes first step to explore how a single neuron behaves and then build it into a system. In particular, the biological neural system has nonlinear and parallel characteristics that is distinguished from those of a conventional von Neumann computer system. Therefore, for the realization of an artificial neural network system, it is necessary to develop a neuromorphic device capable of simulating the synaptic functions with hardware implementation. The learning and memory dynamics at the cellular level are achieved through changes of synaptic connection

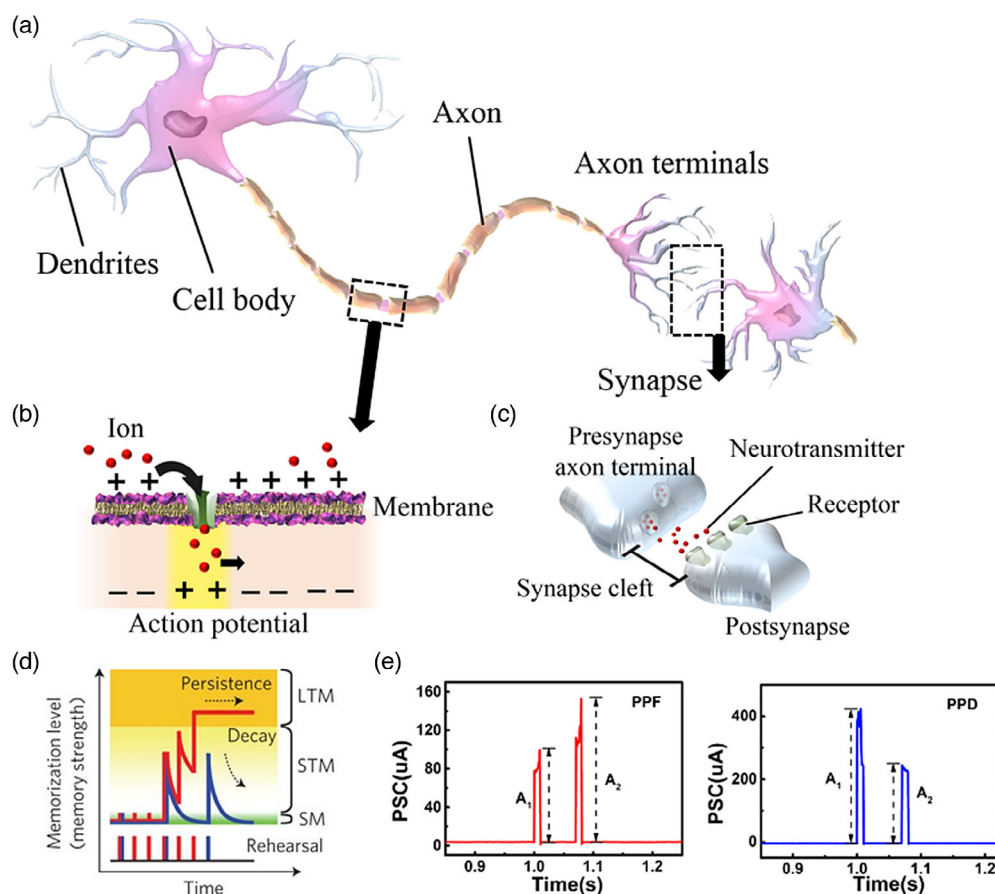


Figure 2. Biological neuron and synapse. Schematic illustration of a) the biological neuron, b) signal transmission process in neuron, and c) synapse between neurons. d) The sort of synaptic plasticity formed between neurons. Reproduced with permission.^[43] Copyright 2011, Springer Nature. e) The PSC tendency in the neural facilitation. Reproduced with permission.^[45] Copyright 2019, Springer Nature.

between neurons, namely synaptic plasticity.^[5] The change of synaptic connection triggered by sensory and stimulating spikes can induce the excitatory/inhibitory postsynaptic current (EPSC and IPSC) in the neuron and continuously strengthening/weakening the its interconnection. Consequently, synaptic plasticity can be classified as short-/long-term and potentiation/depression (STP, STD, LTP, and LTD) (Figure 2d).^[41–44] In particular, neural facilitation/depression, known as paired-pulse facilitation/depression (PPF and PPD), are considered as a sort of the spike-timing-dependent plasticity properties that are indicative of changes in postsynaptic action potential (Figure 2e).^[45–47] Therefore, it is believed that an artificial synaptic device should be able to mimic these neuroplastic behaviors, and detailed device structure of optoelectronic synapse and their application for artificial intelligent system will be discussed later.

3. Hardware Implementation of Transistor-Based Optoelectronic Synapses

3.1. Device Physics and Device Architectures

To date, various transistor-based optoelectronic synapses for hardware implementation of artificial intelligent systems have been steadily developed through the innovative device architectures and desirable material selection. The biological synapses

have multilevel connection strength (analogue synaptic weight) states between adjacent synapses and experience event-dependent switching behavior during biological information processing. This analogue switching phenomena of synaptic weight is named for synaptic plasticity, which is believed in key factor for biological intelligent computing functions of the CNS such as human–brain and the spinal cord. Similarly, all transistor-based optoelectronic synapses must have a multistep conductance states. In addition, the conductance states of optoelectronic synapses should be switchable though optoelectronic means, which must be maintained and stored for a long time. It is called as persistent conductance switching behavior. Those analogue conductance states and persistent conductance switching behaviors are key factor to provide photo-synaptic plasticity and in-memory computing functions to optoelectronics synapse.

Typical transistors without synaptic functions consist of metallic three terminals (gate-, source, and drain electrodes), insulating gate-dielectric layer, and semiconducting channel layer (Figure 3). All transistor-based optoelectronic synapses also have a similar device configuration that includes the essential components of a typical transistor. However, in the case of typical transistor without synaptic function, the channel layer is constructed using crystalline semiconductors without subgap defect states to manufacture high-performance device with high-mobility and high operational stability (Figure 3a).^[48–50] Furthermore, gate-dielectric layer is fabricated using high-quality

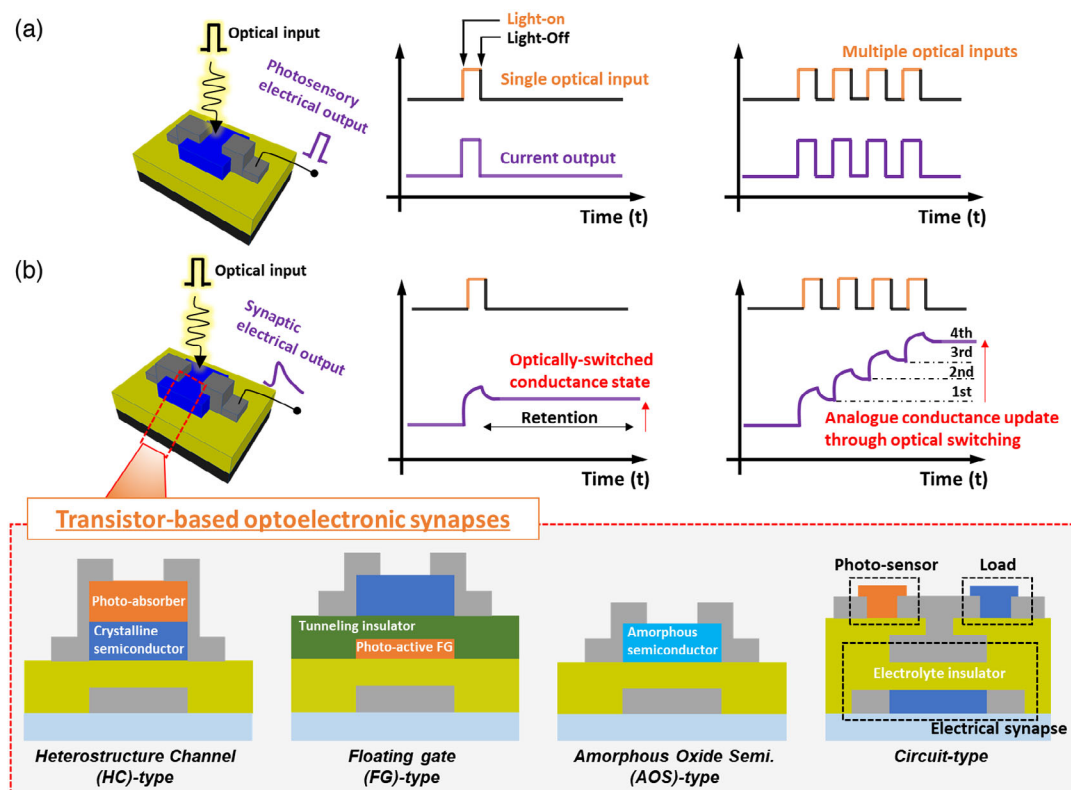


Figure 3. a) Typical crystalline semiconductor-based transistor showing temporary optical conductance switching dynamics without any storage or computing functions. b) Emerging transistor-based optoelectronic synapses showing persistent optical conductance switching dynamics and analog conductance update capabilities with the introduction of additional functional components: HC-, FG-, AOS-, and circuit-type transistor-based optoelectronic synapses.

insulators without internal mobile or fixed charges for hysteresis-free high-performance device. Generally, these transistors experience transient switching of channel conductance only during the lighting period.^[51–53] After optical inputs are terminated, optically switched conductance immediately returns to the original conductance state with fast recovery dynamics. Thus, typical high-performance transistors are suitable to photosensor application which should offer temporary optoelectrical conductance switching behavior without storage function. There are no special resources to storage optically switched channel conductance and perform analogue conductance update. Therefore, the other components should be additionally introduced to develop the transistor-based optoelectronic synapses with photosynaptic function. As shown in Figure 3b, there are four types of the transistor-based optoelectronic synapses designed for hardware implementation of artificial intelligent system; i) heterostructure channel (HC), ii) floating gate (FG), iii) amorphous oxide semiconductor (AOS), and iv) circuit types. Transistor-based optoelectronic synapses, which enable persistent optoelectronic switching and analogue update of channel conductance, can be developed by engineering the materials and structures of the channel and gate insulator layers in conventional transistors. First, in the case of the HC type, the photoabsorber and defective heterointerface are additionally introduced in channel region. Second, in the case of the FG type, photoactive FG layer and insulating tunneling layer are additionally provided between channel and gate insulator. Third, in the case of AOS type, the amorphous semiconductors with numerous photoactive sub-gap states are applied in channel region, instead of conventional crystalline semiconductor. Finally, in the case of circuit type, mobile ions are incorporated into the gate insulator, and this synaptic transistor is interconnected with other functional devices (photosensor and load transistor). Regardless of transistor types, the optical input spike induces the optical conductance switching action (photosynaptic plasticity) to the optoelectronic synapses, creating a postsynaptic current output. Generally, the photosynaptic plasticity triggered by optical input is measured, as the form of EPSC peaks which means excitatory update of channel conductance. It is attributed that optical input mainly offers the positive photoconductivity to channel layer with the generation of photocarriers.^[54–56] However, depending on the type of optoelectronic synapses, they show clear differences in the generation mechanism of photosynaptic plasticity and neuromorphic computing performance such as power consumption, conductance switching linearity, and storage period. Starting in the next section, we describe the unique driving mechanisms and synaptic performance depending on types of transistor-based optoelectronic synapses.

3.2. HC Type

For HC-type transistor-based optoelectronic synapses, the photoabsorber with high optical activity is additionally introduced at the surface regions of high mobility crystalline semiconductor (**Figure 4a**). Here, the photoabsorber provides optoelectronic conductance switching response to optoelectronic synapses.^[57–62] The three types of HC band alignment can be generated when the photoabsorber is stacked onto high-mobility

semiconductor: with straddling gap (type I), staggered gap (type II), and broken gap (type III).^[60–62] Among those HC band alignments, it is regarded that the type-II band alignment is most suitable to implement optoelectronic synapses with high optical responsivity due to sensitive change of channel conductance generated by efficient separation and minimal recombination of photocarriers.^[60] When the optical input with energy exceeding the bandgap of photoabsorber enters, the electron–hole pairs are generated in photoabsorber through band-to-band transition. They are effectively separated into photoelectrons and photoholes near heterojunction. And then, they are separately transported without recombination phenomena, which induces sharp increase in channel conductance (photosensitive EPSC peak) in HC transistor-based optoelectronic synapses. Despite the removal of optical input, the improved channel conductance never immediately come back to original state. Some photocarriers which are trapped at defective heterogeneous interface during optical input can give residual current to channel layer for short term (few seconds to tens of seconds) through thermal detrapping behavior. Thereby, the defective heterogeneous interface makes it possible to maintain the optically increased channel conductance state. However, it quickly returns to its initial state due to the rapid detrapping behavior of the trapped photocarriers. Thus, the photosynaptic plasticity triggered on HC transistor-based optoelectronic synapses reveals volatile retention characteristics, compared with other types. In contrast, it reveals more photosensitive conductance switching operation due to the introduction of high-efficient photoabsorbing layer. Especially, the power-consumption of optical programming operation is proportional to light intensity and illumination area of optical input. Thereby, HC transistor-based optoelectronic synapses appear to be most advantageous to reduce energy-consumption of neuromorphic computing system due to the availability of low-power optical input sources. Moreover, the range of the photoresponse spectrum can also be easily controlled by adopting a custom photoabsorber with an appropriate bandgap.

In fact, HC have been produced through multiple stacking of functional semiconductors with superior carrier transporting and high photoabsorption capabilities.^[57–59] Generally, the crystalline semiconductors such as crystalline oxide, crystalline silicon (c-Si), carbon nanotube (CNT), and layered transition metal dichalcogenide (TMDC) are applied at carrier transport region due to high mobility and low defect density.^[63–65] Next, the photoabsorbers of high-performance solar cells such as perovskite, chalcogenide, and organic semiconductors are additionally used to provide optoelectronic conductance switching response.^[66–68] In addition, the defect interface of the heterojunction region plays a role in generating an analogue memory function and a charge trapping/detrapping phenomenon, which is the origin of synaptic plasticity.^[69,70] Yin et al. reported the HC transistor-based optoelectronic synapse using c-Si nanomembrane (NM) and organic–inorganic hybrid perovskite (**Figure 4b**).^[57] Here, the organolead halide perovskite (MAPbI₃) photoabsorber with visible-light bandgap ($E_g = 1.59$ eV) is introduced in channel region to provide optoelectronic conductance switching function to typical c-Si NM transistor. The Si/MAPbI₃ heterostructure consisting of p-type c-Si and n-type MAPbI₃ is constructed with the type II band alignment which is favorable for sensitive photoresponse and low-power optical programming operation

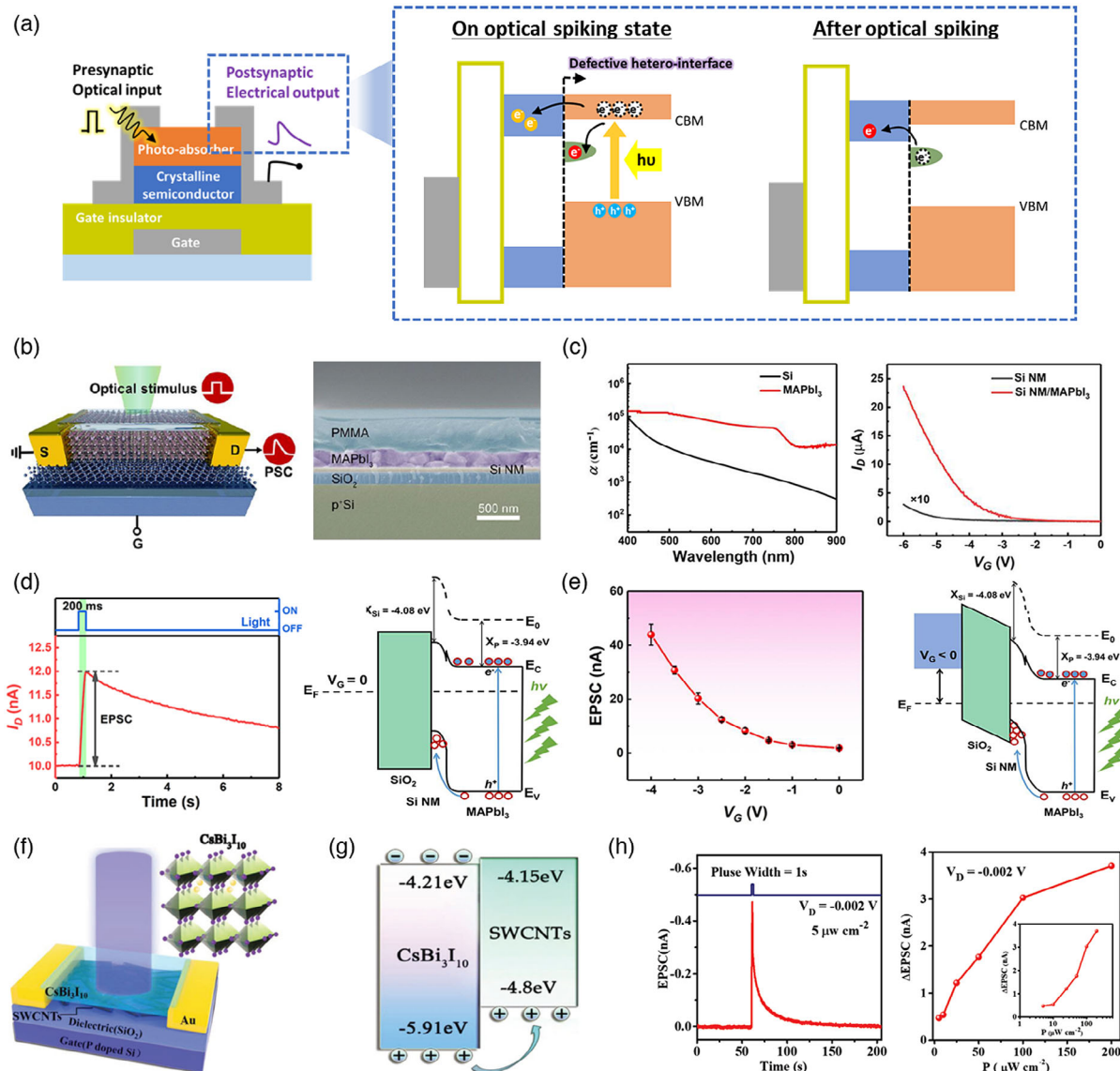


Figure 4. a) HC transistor-based optoelectronic synapses using type II heterostructure of high-mobility crystalline semiconductors and high-efficient photoabsorbers. b–e) HC transistor-based optoelectronic synapse using Si NM/MAPbI₃ perovskite; b) device architecture, c) optical absorption performance of MAPbI₃ and Si NM/ MAPbI₃ heterostructure, d) light-triggered EPSC on Si NM/MAPbI₃ perovskite with type II HC structure, and e) light-triggered EPSCs modulated by gate-bias condition. f–h) HC transistor-based optoelectronic synapse using CNT/CsBi₃I₁₀ perovskite; f) device architecture, g) CNT/CsBi₃I₁₀ with type II HC structure, and h) light-triggered EPSCs. b–e) Reproduced with permission.^[57] Copyright 2020, American Chemical Society. f–h) Reproduced with permission.^[58] Copyright 2019, Wiley-VCH.

(Figure 4c). The electron–hole pairs generated from photoabsorber through band-to-band transition can be effectively separated at heterojunction with the type II band alignment. And then, the photoholes and photoelectrons are effectively transferred along p-type c-Si and n-type MAPbI₃ layers, respectively. It induces a photosensitive switching dynamic of channel conductance, generating strong EPSC peak (Figure 4d). However, it can be maintained for short term due to rapid detrapping behavior of trapped charges at defective heterojunction, showing volatile characteristics with fast decay speed. The optoelectronic synaptic functions such as EPSC, PPF, and short-term/long-term memory (STM/LTM) transition are

successfully mimicked through visible-light spikes due to the use of photoabsorber with visible-light bandgap. Moreover, the EPSC peaks can exquisitely be modulated by constant gate-bias applied to gate terminal. It is due to band bending change of the p–n heterojunction by gate-bias modulation (Figure 4e). However, organic–inorganic perovskite photoabsorber induces device instability issue due to weak environmental durability. Alternatively, HC transistor-based optoelectronic synapses with excellent environmental stability are developed using crystalline CNTs and inorganic perovskite photoabsorber (Figure 4f).^[58] As a inorganic perovskite photoabsorber, the cesium bismuth iodide (CsBi₃I₁₀) photoabsorber with visible-light bandgap

($E_g = 1.70$ eV) is covered on crystalline CNT semiconductor. The CNT/CsBi₃I₁₀ heterostructure consisting of p-type CNT and p-type CsBi₃I₁₀ is constructed with the type II band alignment. Due to CNT/CsBi₃I₁₀ heterostructure with the type II band alignment, the photoholes and photoelectrons are rapidly separated toward CNT and CsBi₃I₁₀, respectively (Figure 4g). Thus, it showed sensitive conductance switching behavior though low-power optical input with weak light intensity (Figure 4h). Similarly, the optically switched conductance of the HC transistor-type optoelectronic synapses disappears rapidly and shows volatile storage properties due to the fast exhaustion of the charges trapped at the heterointerface. As a result, innovative strategies to overcome short retention duration and volatile synaptic plasticity of HC transistor-based optoelectronic synapses must be preferentially be developed.

3.3. FG Type

In the case of FG transistor-based synapses, it can be constructed via vertical multistacking of functional layers including blocking dielectric layer, FG layer, tunneling dielectric layer, and semiconducting channel layer (Figure 5a). FG structure is the most popular device architecture for transistor-based synaptic devices with channel conductance switching functions and long-term retention characteristics, regardless of optoelectronic and electric synapses.^[71–75] In the case of FG transistor-based optoelectronic synapses, the photoactive FG layer with nanoscale dimension is introduced between insulating blocking and tunneling dielectric layers for optical conductance switching response.^[72–74] In addition, high-quality tunneling dielectric layers with large bandgaps and low defect density are required to effectively update the conductance state by preventing recombination between trapped charge carriers and free carriers with opposite polarity. When the optical input with energy exceeding the bandgap of photoactive FG enters, the electron–hole pairs are formed at photoactive FG layer through band-to-band transition. According to the band alignment, the photoholes (photoelectrons) are trapped at FG layer, and the photoelectrons (photoholes) are transferred through the tunneling layer to semiconducting channel layer. Here, the photocarriers which are transferred to semiconducting channel layer contribute on the improvement of channel conductance, inducing the generation of EPSC peak. Next, the optical input is removed, but the charge carriers trapped in the FG layer induce an internal electric field, accumulating free carriers with opposite polarity in the channel region. As long as the carriers trapped in the FG layer do not disappear, the optically updated conductance state can be maintained for a long time (over several ten seconds) due to more free carriers accumulated in the channel layer. Therefore, FG structures provide nonvolatile memory functions with a much longer retention period to transistor-based synaptic devices, compared with other approaches.

Various FG transistor-based optoelectronic synapses have been reported, showing optoelectronic conductance switching behavior for in-memory computing. Generally, the low-dimensional photoabsorbers are applied at the FG region to provide nonvolatile channel conductance switching and optoelectronic responses.^[72–74] For example, the FG transistor-based

optoelectronic synapse using perovskite quantum dots (QDs) photoabsorber with visible-light bandgap is reported, showing photoprogrammable/electric-erasable operation and multilevel conductance states.^[72] Here, inorganic perovskite QD (photoactive FG), thick SiO₂ (blocking dielectric layer), thin poly(methyl methacrylate) (PMMA, tunneling dielectric layer), and pentacene (semiconducting channel) are introduced to individual functional regions (Figure 5b). This FG transistor-based optoelectronic synapse using inorganic CsPbBr₃ QDs revealed light-programmable/electric-erasable memory functions, wide memory window, and superior cyclic operation stability (Figure 5c). The optoelectronic conductance switching and nonvolatile storage dynamic become the basis of light-induced EPSC, bias-induced IPSC, and optoelectronic synaptic plasticity. It can successfully demonstrate EPSC, IPSC, STP, LTP, and SRDP dynamics via optoelectronic means (ultraviolet [UV]-light and positive/negative bias inputs) (Figure 5d). During light-programming step, the numerous photocarriers arise in the perovskite QDs due to desirable bandgap and efficient photoabsorption. Here, photoholes easily move from the CsPbBr₃ to pentacene through tunneling layer due to a bending of energy band. Meanwhile, the photoelectrons captured in the CsPbBr₃ QD induce an internal electric field, accumulating more hole carriers in the semiconductor channel. Despite the removal of the optical inputs, the updated conductance state can be maintained for long-time due to photoelectrons trapped in the CsPbBr₃ QDs, which enables the generation of nonvolatile photosynaptic plasticity dynamics. Furthermore, it flexibly can be returned to initial state using negative gate-bias spikes for the emulation of inhibitory channel conductance switching (Figure 5e). Next, Sun et al. reported FG transistor-based optoelectronic synapses using 2D graphene oxide (GO) surrounded by long alkyl chains with core–shell structure.^[73] The GO nanosheet (photoactive FG), thick polymeric ion-gel (blocking dielectric layer), long alkyl chains (tunneling dielectric layer), and InGaZnO (semiconducting channel) are introduced at individual functional regions (Figure 5f). The processing step for stacking the FG structures can be reduced using the photoactive nanomaterials with the core–shell structure. Here, FG and tunneling dielectric layers can be fabricated by solution-coating GO nanosheets surrounded with long alkyl chains at once. The photoactive alkylated GO provides optoelectronic channel conductance switching function and nonvolatile synaptic plasticity to optoelectronic synapse. The switching response of channel conductance by electrical input becomes more sensitive with the assistance of optical spikes. Synergetic combination of electrical and optical input modes is desirable for power-efficient neuromorphic computing, compared with common electrical operation mode. As a result, the FG transistor-type optoelectronic synapse appears to be the most favorable for the application of neuromorphic in-memory computing due to its stable analogue conductance state and nonvolatile optoelectronic synaptic plasticity. Moreover, the range of the photoresponse spectrum can be easily controlled using custom nanoscale photoabsorbers with an appropriate bandgap. However, complex processing steps and various materials are required, compared with the case of HC and AOS transistor types. Therefore, the task of simplifying processing steps must be carried out steadily for the producing artificial synapses applicable to the industry.

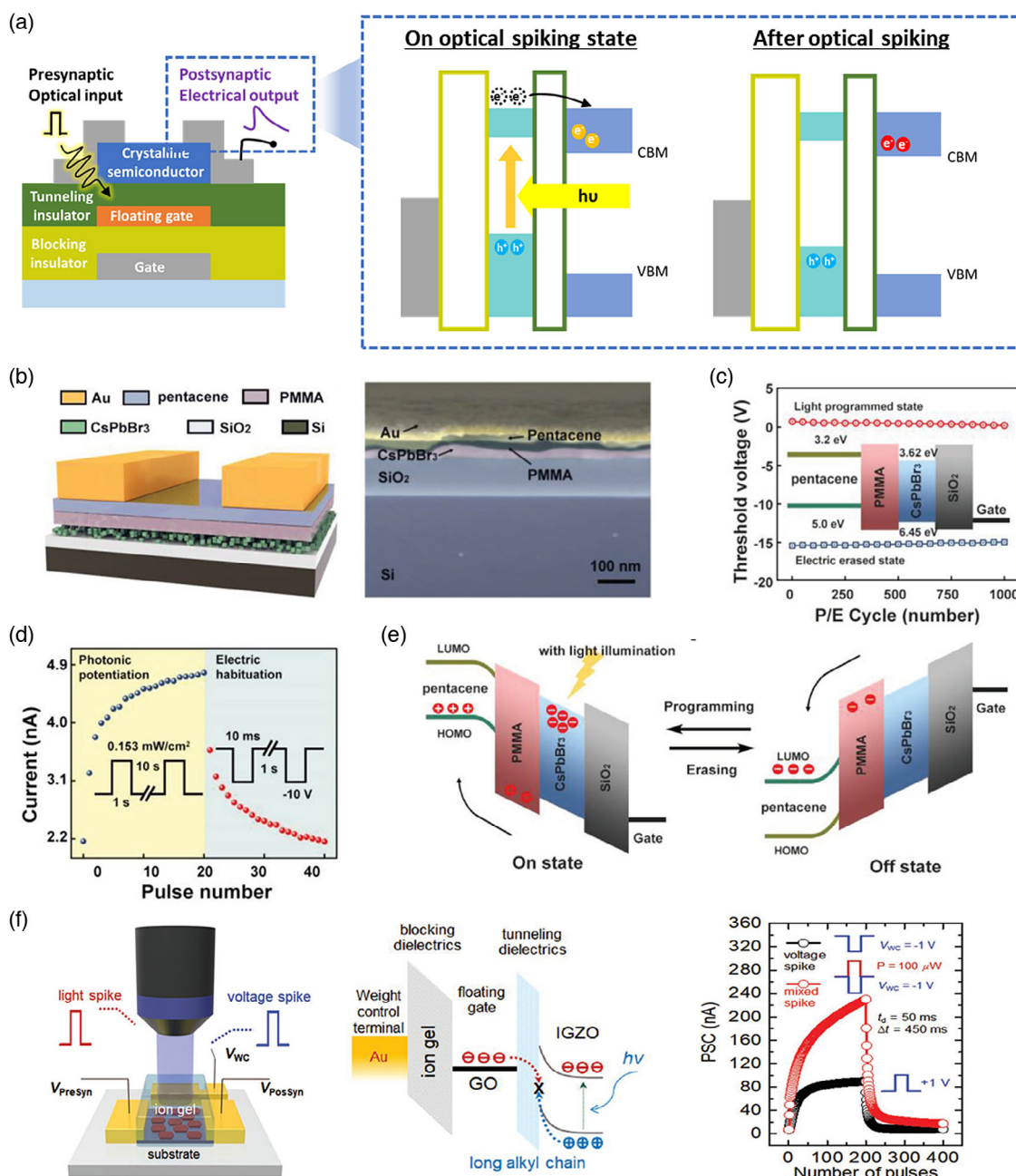


Figure 5. a) FG transistor-based optoelectronic synapses using low-dimensional semiconductors at FG region. b–e) FG transistor-based optoelectronic synapse using inorganic perovskite (QDs); b) device architecture, c) light-programmable and electric-erasable memory functionality, d) photonic excitation and electric inhibition dynamics of synaptic weight, and e) operation mechanism under light programming and electronic erasing states. f) FG transistor-based optoelectronic synapse using alkylated GO nanosheets; device architecture, electric excitation (positive bias) and electric inhibition (negative bias) dynamics of synaptic weight, and power-efficient synaptic weight update through the assistance of optical input spike. b–e) Reproduced with permission.^[72] Copyright 2018, Wiley-VCH. (f) Reproduced with permission.^[73] Copyright 2018, Wiley-VCH.

3.4. AOS Type

Generally, the crystalline semiconductors applied at channel region provide temporary photoresponse with immediate recombination dynamics due to the absence of localized subgap states. Therefore, the simple transistors based on crystalline semiconductors without special device architecture are more

suitable for photosensors with fast recovery dynamics, not optical synapses and memory devices. In contrast, the amorphous semiconductors can provide optoelectronic conductance switching and long-term retention functions to simple transistor due to the existence of numerous localized subgap defect states (Figure 6a).^[76–78] In terms of transistor-based optoelectronic synapse using amorphous semiconductor at channel region,

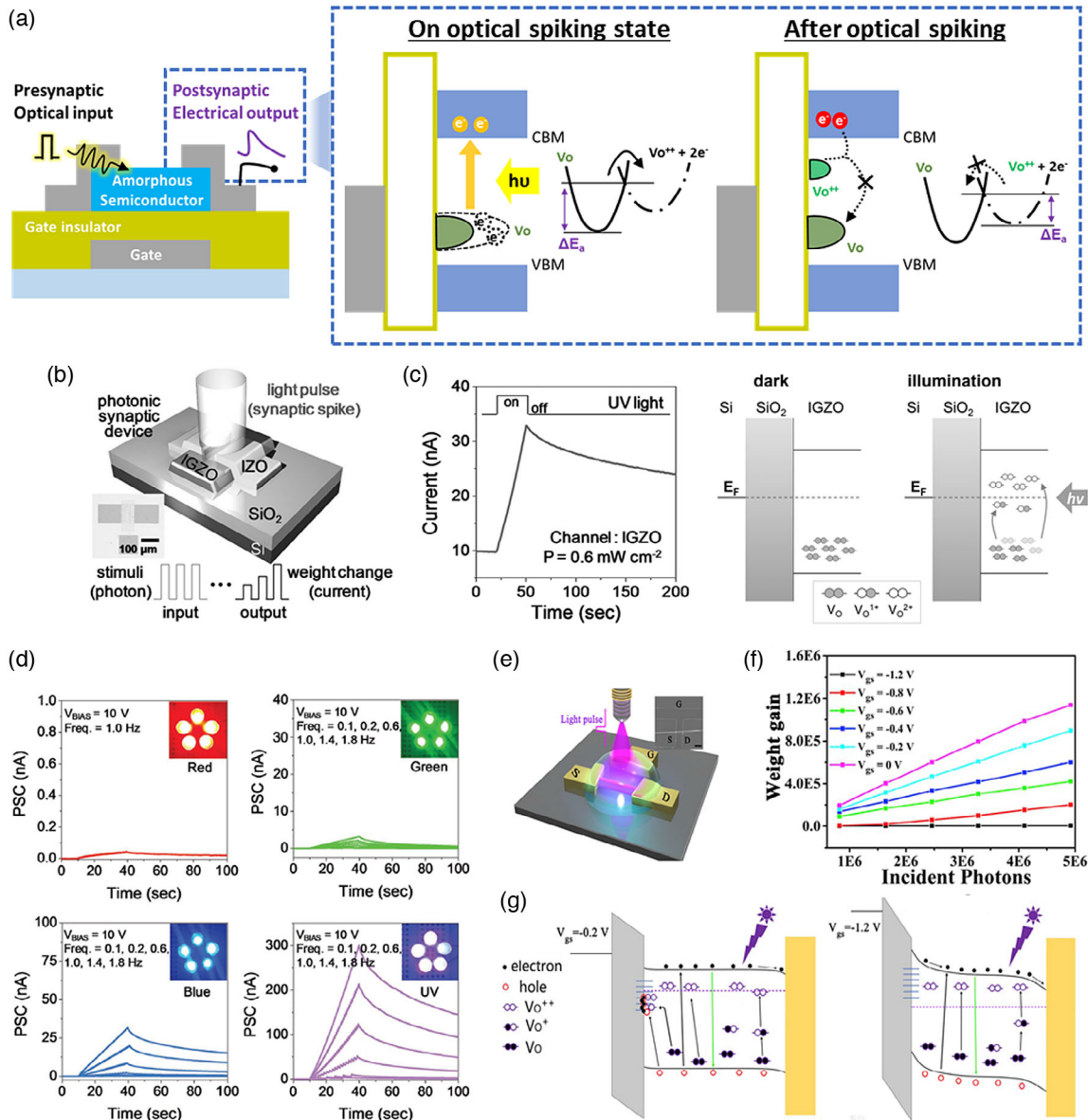


Figure 6. a) AOS transistor-based optoelectronic synapses driven with photoionization mechanism of subgap defect states. b–d) AOS transistor-based optoelectronic synapse using amorphous IGZO semiconductor; b) device architecture, c) optical input-triggered EPSC peak and its generation mechanism, and d) spectrum-dependent EPSC peaks. e–g) SnO₂ NW optoelectronic synapse; e) device architecture, f) gate-bias modulated weight gain, g) the modulation of synaptic plasticity using gate bias terminal and its driving mechanism. b–d) Reproduced with permission.^[76] Copyright 2017, Wiley-VCH. e–g) Reproduced with permission.^[77] Copyright 2019, Elsevier.

AOS has attention due to its unique persistent photoconductivity (PPC) phenomena that the light-induced conductance state steadily remains despite the removal of optical input. AOSs are representative amorphous semiconductor materials with numerous subgap states.^[79–81] Among various point defects including oxygen vacancy (V_o), metal vacancy, interstitial oxygen, interstitial metal, oxygen antisite, and metal antisite, the V_o defects are most preferentially generated due to their low formation energy in most AOS materials.^[82–84] They introduce localized trap states at deep subgap region near valence band maximum (VBM). When the optical input enters the AOS,

V_o -induced deep trap states enable to offer photoelectrons and photoionized V_o ions (V_o^+ and V_o^{++}) to AOS channel layer through the photoionization reaction, not band-to-band transition.^[85,86] Those photoelectrons increase channel conductance of AOS optoelectronics synapse, inducing the generation of EPSC peak. Even if the optical input is removed, the photoelectrons never rapidly disappear via recombination process. The increased channel conductance can be maintained for a long time without special device architecture. This is because the recombination between photoelectrons and photoionized V_o ions is a nonspontaneous process that requires high activation energy.

Thus, AOS transistor-type optoelectronic synapses can demonstrate nonvolatile optoelectronic synaptic plasticity based on photoionization and nonspontaneous recombination dynamics of point defects.

Emerging AOS-type transistor-based optoelectronic synapses have been reported, showing optoelectronic channel conductance switching behavior and nonvolatile synaptic plasticity function without complex structural design. For example, Lee et al. developed the AOS transistor-based optoelectronic synapses that allow nonvolatile optoelectronic switching of the channel conductance in conventional transistor configuration (Figure 6b).^[76] Various In-, Zn-, and Sn-based oxide semiconductors such as InGaZnO (IGZO), InZnO, InSrZnO, and ZnSnO can be fabricated with amorphous phase due to their complex composition at low-temperature process condition.^[79–81] Those AOS films include various point defects due to inferior bonding networks of metal cations and oxygen anions. As already mentioned, the optical switching of the channel conductance can be triggered due to photoionization of V_o by UV input, resulting in EPSC peak. Due to the nonspontaneous recombination kinetics of photoionized V_o defects (V_o^+ and V_o^{++}) and photoelectrons, they remain for a long-time despite the removal of optical input, showing the nonvolatile conductance retention properties (Figure 6c). Various synaptic functions such as EPCS, STM, LTM, and STDP can be demonstrated based on nonvolatile conductance switching dynamics by the photoionization of V_o defects. Compared with other types, it is advantageous for high-density integration and simple fabrication of optoelectronic synapses due to relatively simple device configuration. However, they show photoinensitive conductance switching performance, as a small amount of photocarriers are usually created by photoionization of V_o defects. Thus, it requires the more powerful optical input sources with high light intensity, which is disadvantageous for building power-efficient optoelectronic computing systems. Furthermore, it reveals the meaningful conductance switching dynamics and EPSC peaks in the limited spectral range (energetic visible [blue] to UV light) because the V_o defect states are positioned at the deep subgap region (2.2–2.8 eV under conduction band minimum [CBM]) (Figure 6d).^[85,86] Therefore, the several strategies have been proposed to improve the photoconductance switching performance of AOS transistor-type optoelectronic synapses. First, the approach applying constant bias at gate-bias terminal is achieved to modulate optically triggered synaptic weight of AOS transistor-type optoelectronic synapses (Figure 6e).^[77] This optoelectronic synapse using SnO nanowire (NW) shows UV-light programmable and gate bias adjustable characteristics (Figure 6f). The more positive bias conditions resulted in the accumulation of more photoelectrons in the channel layer by the favorable bending properties of the band alignment, showing more photosensitive conductance switching dynamics (Figure 6g). Next, the approaches controlling V_o concentration in AOSs are proposed through composition engineering.^[78] The V_o concentration can dramatically increase by lowering compositional ratio of metal cations (Ga and Sn) with high oxidation power. It was identified that V_o -rich IGZO with In-rich and Ga-poor configurations provide several ten times higher photoresponse to AOS transistor-type optoelectronic synapses, compared with the case using V_o -poor IGZO with In-poor and Ga-rich configurations.

However, implementing low power photoprogrammable optoelectronic synaptic systems using AOS-type transistors is still restrictive due to the low photoresponse. In addition, it is difficult to create an optoelectronic synaptic system operable in a wide spectrum ranges because the photoionization reaction of V_o -induced subgap states can occur limitedly by energetic optical inputs with short wavelength. Therefore, innovative techniques that can generate more subgap states and shallow traps in AOSs must be developed to implement power-efficient optoelectronic neuromorphic systems with high optical sensitivity and wide-spectral response.

3.5. Circuit Type

In addition to aforementioned single-device-type optoelectronic synapses (HC, FG, and AOS-type transistor based), the circuit-type transistor-based optoelectronic synapses have been steadily developed for artificial intelligent systems. The single-device-type optoelectronic synapses can directly convert the presynaptic optical input to postsynaptic electrical current output. The optical response and channel conductance switching dynamics for the emulation of photosynaptic plasticity are simultaneously accomplished in single device. In contrast, the circuit-type transistor-based optoelectronic synapses are constructed by interconnecting several device components that perform discrete functions: photosensor, load transistor, and electrical synapse (Figure 7a).^[87–89] They can demonstrate optoelectronic conductance switching actions through a multistep sequence of human-like visual information processing: optical input, photo-to-bias conversion, synaptic current output. Individual photosensor (artificial retina), load transistor (artificial optic nerve), and electrical synapse (artificial brain) are responsible for the absorption of the optical input spike, the conversion of light-to-bias signal, and the generation of synaptic currents, respectively.

When the optical input is applied to the entire region, the load transistor and electrical synapse seldom reveal direct optical interaction due to the absence of photosensitive elements. In contrast, the photosensor with crystalline photoabsorber experience conductance change by reception of the optical input. However, it is maintained only during the illumination period and there is no storage function, so it disappears immediately when the incident light is removed. Instead, the photovoltaic divider consisting of photosensor and load transistor provide proper electrical bias spike to voltage node region during the illumination period through the conversion processing of light-to-bias signal. The amplitude of the bias signal applied to the voltage node is proportional to the conductance state of the optical sensor that is switched by the optical input. This bias spike signal is transmitted to the gate terminal of the electrical synapse along the wire interconnected with the voltage node region of the photovoltaic divider. Next, when the converted bias spike arrives, the state of the channel conductance of the electrical synapse is switched due to the drift motion of the mobile cations included in the electrolyte insulator. Many mobile cations are accumulated near the interface of channel layer and electrolyte insulator. The drift motion of mobile cations by bias input spike induces the channel conductance switching behavior with the concentration change of free carriers. Even if the bias spike provided by the photovoltaic divider is terminated, the updated conductance state

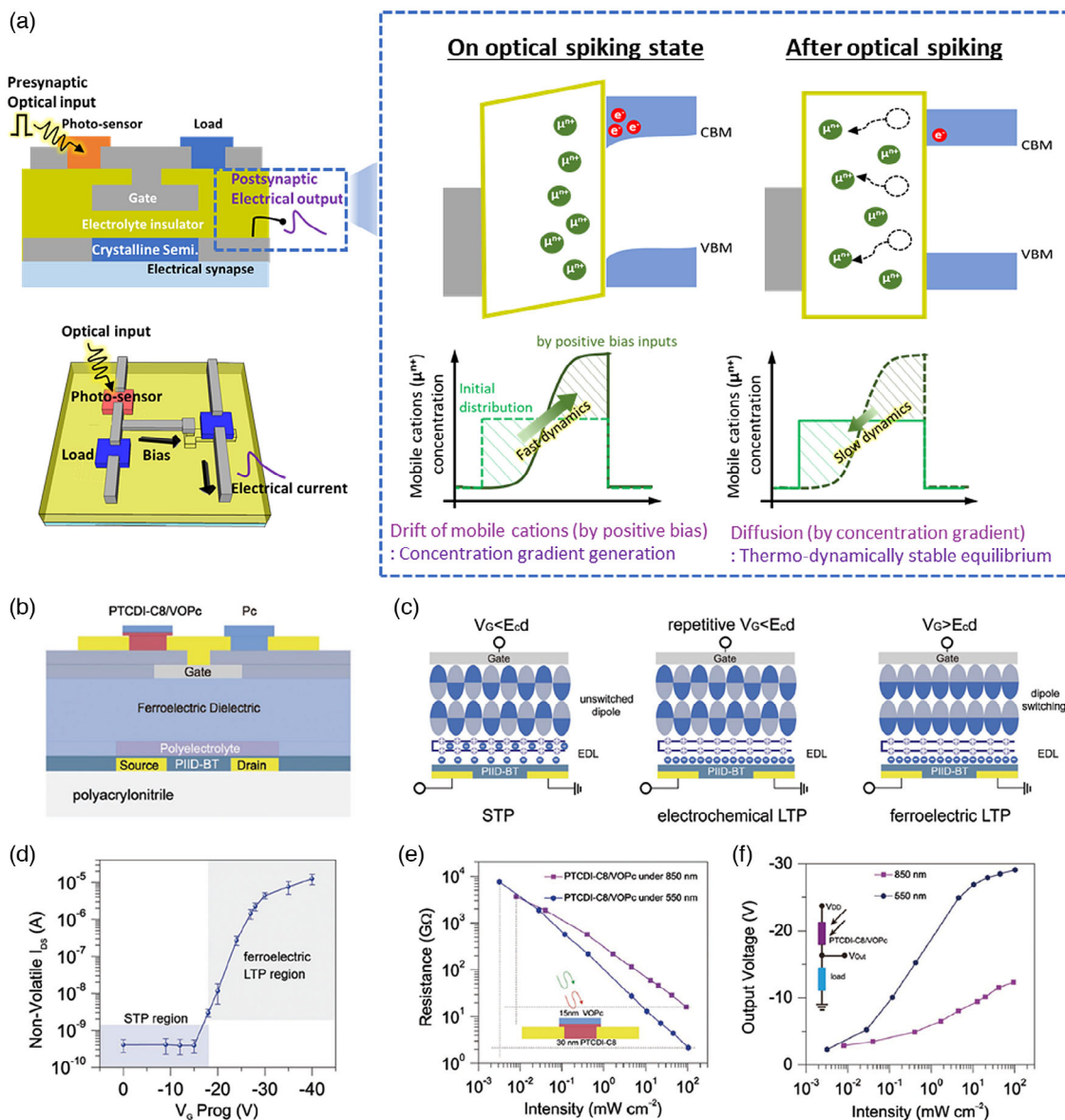


Figure 7. a) Circuit configuration (cross-sectional and planar views) and driving mechanism of circuit-type transistor-based optoelectronic synapse. b–f) Circuit-type optoelectronic synapse including organic ionotronic transistor with solid electrolyte insulator [P(VP-EDMAEMAES)]; b) circuit configuration, c) driving state of ionotronic transistor-based electrical synapse depending on applied bias conditions, d) EPSC dependent on the programming voltage, e) channel conduction change of organic photosensor by optical inputs (550 and 850 nm), and f) photoconverted voltage signal in the photovoltaic divider. b–f) Reproduced with permission.^[88] Copyright 2018, Wiley-VCH.

can be maintained due to the slow recovery motion of the accumulated metal cations near interface region, showing synaptic plasticity behavior. As a result, the circuit-type transistor-based optoelectronic synapses can carry on optoelectronic synaptic plasticity functions based on photo-to-bias conversion of photovoltaic divider and electrical conductance change of electrical synapse.

For the implementation of circuit-type optoelectronic synapses, the photosensor, load transistor, and electrical synapse are integrated on same substrate and interconnected using electric wires. The photosensors are produced by applying the following

crystalline photoabsorbers to the channel layer: perovskite, chalcogenide, and organic semiconductors. Next, load transistors are fabricated using following high-mobility crystalline semiconductors to the channel layer; crystalline oxide, c-Si, CNT, and TMDC semiconductors. Next, the ionotronic transistor using a high-capacity electrolyte insulator in the dielectric layer is utilized as a transistor-based electrical synapse.^[90–93] The electrolyte insulator for ionotronic transistors consists of insulating matrix and mobile cations. The proton (H^+), alkali (Li^+ , Na^+ , and K^+), and alkaline-earth metal ions (Ca^{2+} and Mg^{2+}) with small ionic radii can be used as mobile cations in electrolyte insulator. According

to matrix phase, electrolyte insulators can be classified to following types: liquid-type (ionic liquid), gel-type (ion gel), and solid-type (polyelectrolyte and inorganic electrolyte).^[94–97] In the case of simple transistor-based electrical synapses without optical responses, the ionotronic transistors have been mostly constructed using fluidic ion-liquid and sticky ion-gel-type electrolytes. Aqueous solvents and gel-polymers such as PMMA, polyacrylonitrile, and poly(vinylidene fluoride-co-hexafluoropropylene) are mainly utilized, as a matrix material of ion liquid and ion gel electrolytes.^[94] However, those liquid and gel electrolytes are not suitable for fabricating photosensors, load transistors, and ionotronic transistors together on the same substrate due to their inferior mechanical properties. Instead, ionotronic transistors which contain the robust solid electrolytes such as poly(ethylene oxide) (PEO), poly(vinyl phosphonic acid-co-acrylic acid) P(VPA-AA), poly[(1-vinylpyrrolidone)-co-(2-ethylmethacrylate ethyl sulfate)] [P(VP-EDMAEMAES)], and sodium β -alumina are promising, as electrical synaptic part of circuit-type optoelectronic synapses.^[94] For example, Wang et al. reported the circuit-type optoelectronic synapse including the photosensing, photo-to-bias converting and synaptic computing components (Figure 7b).^[88] Especially, the transistor-based electrical synapse without optical responsivity is fabricated using solid-state polyelectrolyte and ferroelectric polymer at gate dielectric and photo-insensitive p-type copolymer at the channel layer. The organic synaptic transistor provided the STP, and the electrochemical LTP, and ferroelectric LTP according to the amplitude of gate bias (Figure 7c). In the case of applying repetitive gate bias lower than coercive field of ferroelectric polymer [P(VDF-TrFE)] to gate terminal of organic electrical synapse, the mobile ions in polyelectrolyte [P(VP-EDMAEMAES)] drift toward channel interface. And then, it induces a nonvolatile weak current increase, triggering the electrochemical LTP. Further, when applied gate bias exceeds coercive field of ferroelectric polymer, the electric double layer of ferroelectric polymer allows the ferroelectric LTP due to its large capacitance value, resulting in the nonvolatile strong ferroelectric LTP. By integrating organic electrical synapse with organic photovoltaic divider, the circuit-type optoelectronic synapse can be achieved (Figure 7d). Meanwhile, the organic photovoltaic divider consists of organic photosensor and organic load transistor, converting external optical input to bias output. The organic photosensor experiences conductance change by optical inputs (Figure 7e). Instantly, the photovoltaic divider provides corresponding light-converted bias spike to the gate terminal of electrical synapse (Figure 7f). In addition, circuit-type optoelectronic synapse shows promising potential as spectrum-selective memorizing platform of various image patterns. On circuit-type optoelectronic synapse, it is available to successfully demonstrate retina-like computing processing of visual information. However, it has the disadvantage of low device density and complex processing, compared with emerging single-device-type optoelectronic synapses. In addition, electrical synapses driven using diffusive mobile cations provide nonlinear switching performance of the conductance state, which reduce the recognition accuracy of image patterns for neuromorphic computing.^[59,98] Therefore, innovative technologies for compact fabrication and linear conductance switching performance of circuit-type optoelectronic synapses must be continuously developed to

implement high-density and high-performance artificial intelligent systems.

4. Advanced Application for Neuromorphic Computing System

The main research objective of the neuromorphic electronics is hardware implementation to emulate in-memory computing functions of a biological brain, enabling to learn, memorize, and recognize massive and unstructured data through parallel and power-efficient ways. In addition to the basic synaptic features mentioned in Section 3, there are also notable advanced functions for neuromorphic computing system; i) Boolean logic gate and ii) associative learning. This section describes advanced applications related to artificial intelligent computing systems using optoelectronic synapses.

4.1. Boolean Logic

In addition to memory and calculation functions, logic operations are a key component of the computing system for information processing. Recently, innovative logic gates using optoelectronic synapses have been developed for advanced neuromorphic in-memory computing.^[69,99] Ahmed et al. reported optical logic gate using layered black phosphorus (BP) optoelectronic synapse with bipolar photosynaptic plasticity.^[99] Interestingly, BP optoelectronic synapse provides a negative photocurrent under 365 nm illumination due to the dissociation of surficial ambient oxygen introducing localized charge trap sites on the surface of BP. In contrast, it offered positive photocurrent under 280 nm illumination (Figure 8a,b). Thus, BP optoelectronic synapse can perform both EPSC and IPSC functions using two types of UV lights with different wavelengths (280 and 365 nm) (Figure 8c). The time-dependent sequential updates of EPSC and IPSC peaks based on photosynaptic plasticity dynamics are successfully realized though paired optical spikes (Figure 8d). As the optical logic gate, two series-connected BP devices are integrated. For an exclusive OR (XOR) logic gate operation, different spectral lights are applied to optical logic gate as input A and input B (Figure 8e). When both optical inputs are OFF [0–0] and ON [1–1] states, the channel conductance remains in initial state and corresponds to OFF state [0]. In contrast, when either of the two inputs is ON state, the channel conductance experience dramatic change and corresponds to ON state [1]. The result of the calculation between the input signal and the output signal matches the XOR logic. Next, for an OR logic gate operation, same spectral lights are applied as input A and input B (Figure 8f). When either or both of optical inputs are ON, it provides an output signal [1]. The result of the calculation between the input signal and the output signal matches the OR logic.

4.2. Association Learning

The association learning means that conditioned stimulus becomes paired with an unconditioned stimulus by repetition of pairing. In Pavlov's dog experiment which is the representative example of association learning process, the feeding food

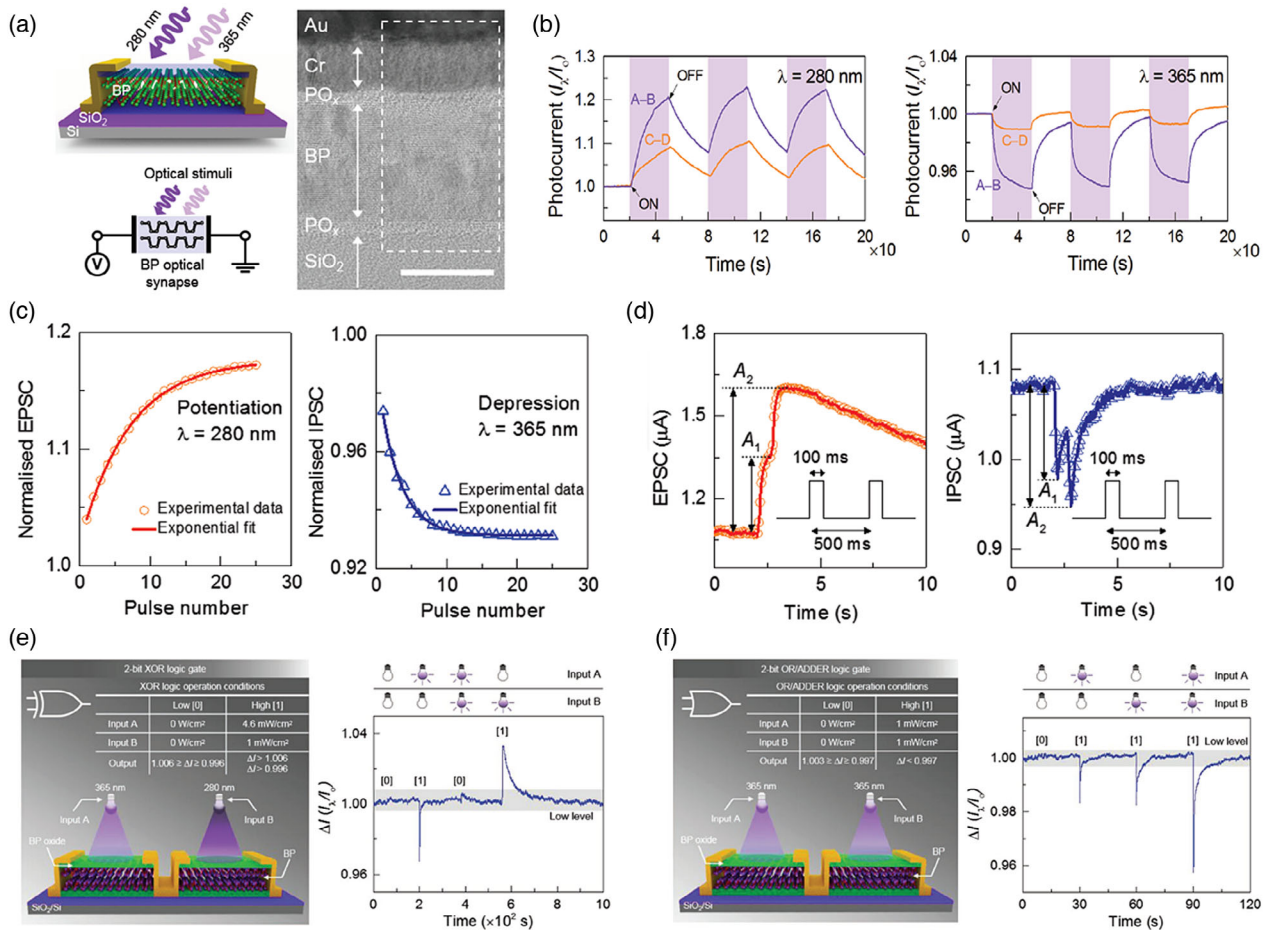


Figure 8. Optical logic gate using BP optoelectronic synapse with bipolar photosynaptic plasticity. a) Device scheme, b) bipolar photoresponse (positive and negative photocurrent generation), c) EPSC and IPSC behaviors, d) PPF functions, and optical logic gates of e) XOR and f) OR functions. a–f) Reproduced with permission.^[99] Copyright 2019, Wiley-VCH.

and bell-ringing inputs were chosen as a role of unconditioned (US) and neutral/conditioned stimulus (NS/CS) for salivation. Initially, only the US activates the unconditioned response (UR; here, salivation). After association formation through repeated training, the CS alone can lead the conditioned response (CR) of salivation. This CR can be obtained by associative learning processes.

Generally, conventional electrical synapses have demonstrated all electrical input-driven associative learning modeling using two-types of electrical spikes (strong and weak bias spikes).^[100,101] In contrast, several surveys begin to successfully report photosynaptic devices to enable to mimic association learning using all-photonic (two optical spikes with different spectrum) or optoelectronic hybrid (one electrical and one optical spikes) input modes.^[69,102,103] Cho et al. reported HC transistor-based optoelectronic synapse which can demonstrate associative learning using all-photonic inputs (Figure 9a).^[69] Here, heterostructure is constructed using ZnSnO (ZTO) with UV-light bandgap ($E_g = 3.7$ eV) and CdS photoabsorber with visible-light bandgap ($E_g = 2.3$ eV). Thus, ZTO/CdS HC with broadband photoabsorption properties from UV to visible-light regions provide spectrum-sensitive conductance switching properties

for HC transistor-based optoelectronic synapse. When optical input enters HC-type transistor-based optoelectronic synapse, most photocarriers are separated near heterojunction and transported along ZnSnO and CdS, contributing on the increase in channel conductance and generation of EPSC peak. The UV-light input can provide stronger EPSC peak and conductance change for optoelectronic synapse due to more generation of photocarriers, compared the case of green-light input. It is because the UV light input can be absorbed by both ZnSnO with UV-light bandgap and CdS with visible-light bandgap. In contrast, the weakest EPSC peak is monitored under green-light input. This is because green-light can be limitedly absorbed in the CdS layer with visible-light bandgap, except for the ZTO layer with UV-light bandgap. Thereby, the UV-light input is used as the optical US, resulting in enough EPSC that exceeds the threshold of postsynaptic response. In contrast, green-light input is introduced as NS/CS (corresponding to ringing), giving weak EPSC below the postsynaptic response threshold before associative learning due to the generation of small amounts of photo carriers. Initially, UV-light spikes (US) can activate postsynaptic response with weight change over threshold of salivation. However, the green-light spikes on neutral state failed to generate salivation

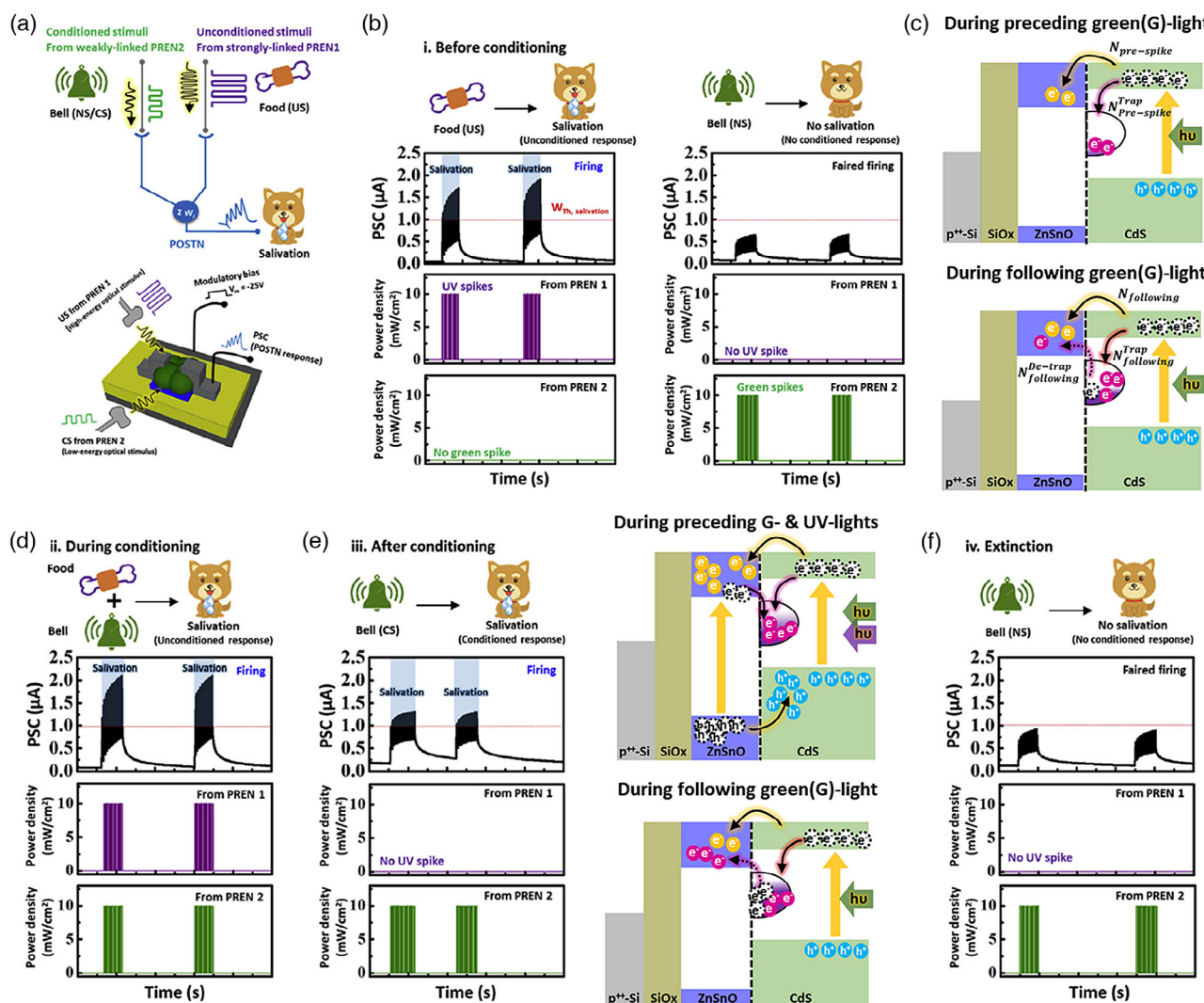


Figure 9. Optoelectronic synapse with association learning function. a) Device scheme and demonstration condition for photosynaptic transistor with oxide/chalcogenide heterostructure (ZnSnO/CdS) channel architecture. b–f) All optical input-driven associative learning process using UV (US) and green (NS/CS) optical inputs; b) before conditioning step, c) weak conductance update action by repetitive green-light inputs, d) during conditioning step, e) strong conductance update action by repetitive green-light inputs after conditioning step, and f) extinction step. a–f) Reproduced with permission.^[69] Copyright 2019, Elsevier.

response due to lower conductance change than salivation threshold value (Figure 9b). Interestingly, the repetitive optical input spikes can induce continuous channel conductance update with detrapping of trapped photocarriers at defective heterointerface (Figure 9c). Nevertheless, green-light inputs still never approach to threshold level for salivation response due to low concentration of detrapped photocarriers from heterointerface. In contrast, the association formation through synergetic training of bell ringing (NS) and feeding food (US) stimuli exchange a role of bell ringing from NS to CS (Figure 9d). Here, the regular training of UV-light and green-light spikes makes temporary association between bell-ringing stimuli and salivation response via synergetic synaptic weight updates. The binary (UV and green) optical inputs offer strongest EPSC peak and conductance change due to generation of high photocarriers concentration, compared the cases of single spectral input. During association conditioning by binary

(UV and green) optical inputs, numerous photocarriers experience charge-trapping dynamics at defective heterointerface. In this moment, the defect states which are positioned at heterointerface region will be fully filled with trapped photocarriers. After association conditioning, the following green-light input can provide stronger EPSC peak due to the optical detrapping behavior of the trapped carriers in the heterojunction region, compared with original EPSC peak generated by the green-light input (Figure 9e). Thereby, green inputs (CS) after association conditioning can lead postsynaptic response for a while due to enough weight change exceeding threshold of salivation. However, if only CS is restrictively repeated without further association learning, the amplitude of EPSC peak triggered from green-light input go back to the original level with rapid exhaustion of the carriers accumulated at defective heterointerface. Thus, the temporary association between green-light input (bell ringing) and postsynaptic

response (salivation) go back to initial weak synaptic interconnection (Figure 9f).

Next, John et al. reported transistor-based optoelectronic synapse using 2D MoS₂ single-layer semiconductor channel which can execute associative learning function using optoelectronic hybrid input modes (one electrical and one optical spikes).^[103] The MoS₂ optoelectronic synapse holds multiple synaptic plasticity modes, as following: electrical, ionotronic, and optical modes. Three synaptic plasticity modes are due to charge trapping and detrapping at channel/dielectric interface, drift-diffusion of mobile ions in the ion-gel dielectric, and slow recombination of photocarriers. Here, the optical mode input results in strongest EPSC output exceeding threshold of postsynaptic response, whereas the electric mode provides weak EPSC below threshold. Thereby, optical pulses are used as US for postsynaptic response. In contrast, bias pulses applied at the gate terminal are introduced as NS/CS for postsynaptic response. Finally, the association learning modeling using optoelectronic inputs can be successfully achieved on MoS₂ optoelectronic synapse with multiple synaptic plasticity modes.

5. Advanced Application for Artificial Sensory System

Recently, beyond neuromorphic computing application, optoelectronic synapses are applied to implement following human-like artificial optoelectronic sensory system; biomimetic optical nerve, optogenetics, and optical sensorimotor. Especially, the neuromorphic optoelectronics based on optoelectronic synapses will enable the recognition, memorization, and computing processing of incident visual information from external environment, which will be continuously developed toward next-generation humanoid robotics and neuroprosthetics. In this section, we will focus on the recent reports for optoelectronic neuromorphic sensory system and their biomimetic applications that responds to visual information.

5.1. Visual Perception System

Artificial visual perception systems have been implemented using optoelectronic synapses with the form of single devices and circuits. Here, the circuit-type optoelectronic synapses are constructed by interconnection of photosensors, artificial electrical synapse, and/or photovoltaic converters. They can successfully emulate subsequential biological processing procedure of visual information: the reception (retina), transmission (optical nerve), and memory (visual cortex of human-brain).^[87–89] Recently, beyond typical in-memory computing processing of visual information, the retina-inspired advanced image processing functions have been realized through innovative works based on optoelectronic synapses, as following: selective amnesia,^[104] light-adaptable image recognition,^[87] and color pattern recognition.^[87,89] Yu et al. reported an optoelectronic synapse capable of “selective amnesia and memory” behaviors. The selective attention feature allows filtering of wanted spectral information from complex visual images.^[104] As single-device-type visual perception platform, the HC transistor-based optoelectronic synapse was fabricated using high-mobility oxide semiconductor (p-SnO_x/n-IGZO) and organic photo-absorber (PEDOT:PSS)

(Figure 10a). It provided broadband photoabsorption and sensitive photoresponse due to organic photoabsorber with visible-light-level bandgap (Figure 10b). Here, the photosynaptic plasticity triggered from various spectral optical inputs is due to the photoionization reaction of V_O, enabling various neuromorphic computing processing of visual images. Moreover, the optoelectronic synapse can achieve “selective amnesia and memory” behaviors by modulating constant gate bias applied to gate-terminal (Figure 10c). Depending on the modulation state of gate bias, incident image information on optoelectronic synapse can be selectively remembered (i.e., a moth) and forgotten (i.e., a dragonfly). Next, Kwon et al. reported circuit-type optoelectronic synapses which can mimic “photopic and scotopic adaptation” functions of biological retina for environment-adaptable image recognition.^[87] This circuit-type optoelectronic synapses consists of photovoltaic divider and ionotronic synaptic transistor, which corresponds to an artificial retina part and an artificial optic nerve and brain part, respectively (Figure 10d). The ionotronic synaptic transistor is constructed by applying oxide semiconductor (IGZO) to channel layer and solid inorganic electrolyte (Na; Al₂O₃) containing mobile cations to the gate dielectric layer. Here, the photosensor and load transistor of photovoltaic divider carry out direct reception and photo-to-bias conversion operation of visible-light inputs (Figure 10e). The CdSe photosensor with good photoresponsivity enables full color and sensitive image recognition. The converted bias from the photovoltaic divider is proportional to the intensity of the incident light. And then, it is transmitted to the gate terminal of the ionotronic synapse (Figure 10f). Only bias spikes above a certain threshold can raise meaningful postsynaptic current to the ionotropic synapse. By modulating bias condition of load transistor, visual threshold level to provide meaningful postsynaptic current can be controlled (Figure 10g). High bias condition of load gate improves visual threshold level for image recognition (photopic adaptation). Therefore, image pattern including bright surrounding noise can be much clearly classified on optoelectronic synapses array applying photopic adaptation condition (Figure 10h). In contrast, low gate voltage condition suppressed visual threshold level (scotopic adaptation). Therefore, faint image pattern could be much distinctly recognized in optoelectronic synapses array with photopic adaptation states (Figure 10i).

5.2. Optoelectronic Sensorimotor System

In addition to visual recognition, the optogenetics have been proposed to control the biological tissue with optical stimulation to realize soft robotics and neurorobotics.^[105] Recently, optical wireless communicated manipulation of a batoid fish robot made of biological tissues by transplanting the rat’s cardiomyocytes that respond to light guidance has accelerated the realization of optogenetics. In addition to the biological approach of optogenetics, a bioinspired electronic systematic approach also has been proposed for the implementation of electronic prostheses. In this regard, Lee et al. proposed the stretchable optoelectronic sensorimotor synapse system.^[106] In the biological system, the engineered neurons through optogenetic means generate action potentials under light stimulation and delivers a neurotransmitter to a neuromuscular junction in muscle fibers, resulting in

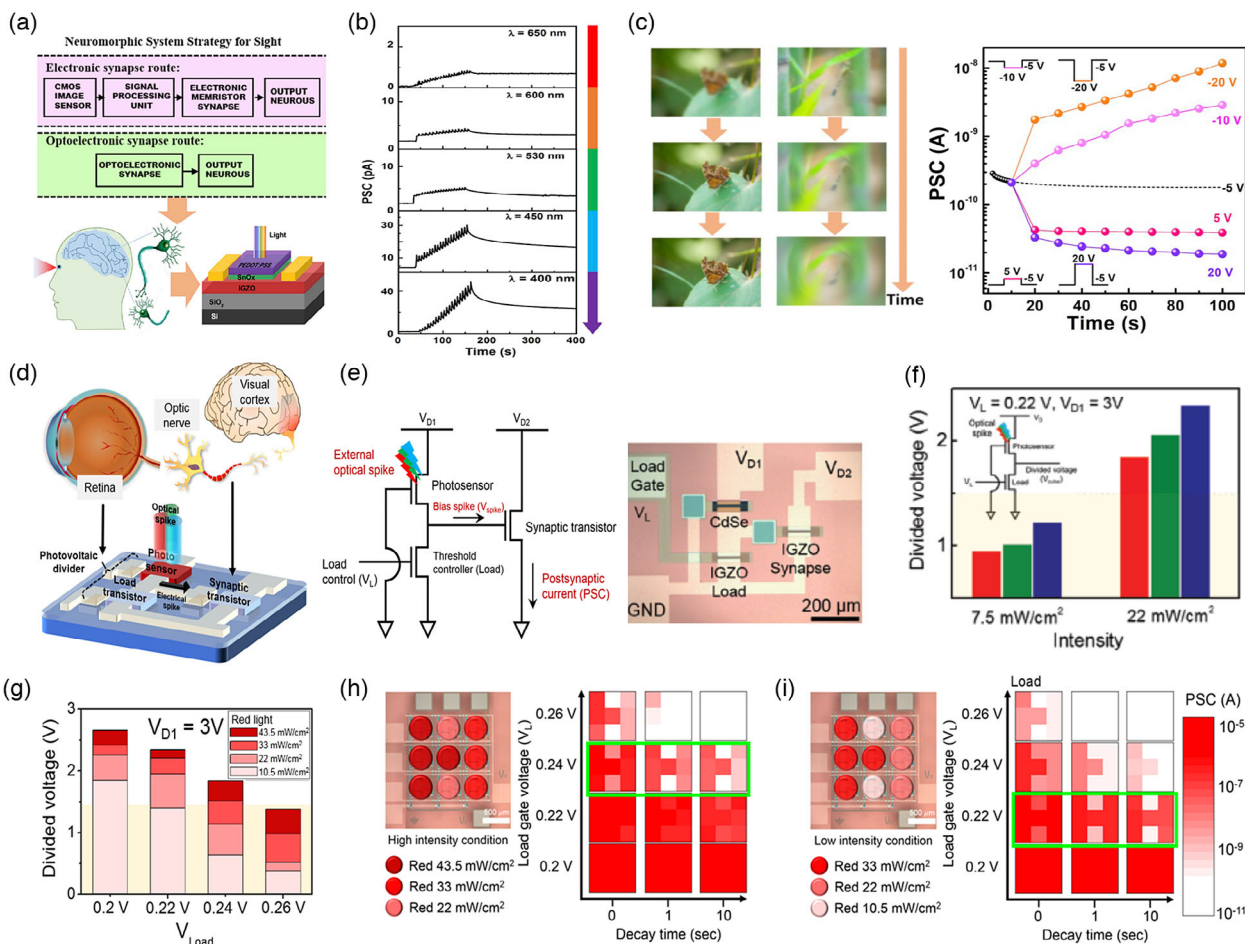


Figure 10. Optoelectronic synapses with retina-inspired advanced image processing functions for artificial visual perception system. HC transistor-based optoelectronic synapse with selective visual perception capability; a) device scheme, b) full-color-triggered EPSC peaks, and c) image processing results using “selective amnesia and memory” function. Circuit-type optoelectronic synapse with light-adaptable visual perception capability; d) The configuration of biological and retina-inspired vision perception systems, e) circuit scheme, f) optical-to-electrical converted voltage (V_{spike}) from the photovoltaic divider under visible-light input, g) visual threshold level controlled through the modulation of load gate bias, and image processing results through h) photopic and i) scotopic adaptation condition. a–c) Reproduced with permission.^[104] Copyright 2019, Elsevier. d–i) Reproduced with permission.^[87] Copyright 2019, Wiley-VCH.

muscle contraction (Figure 11a). Analogously, in an artificial sensorimotor synapse, the optical spike evokes a photodetector to generate output action potential. Then, the electrical postsynaptic bias induces the activation of an actuator as the artificial muscle (Figure 11b). To provide the neuromorphic operation, the organic synaptic transistor showed the increasing EPSC value dependent on spike number as the neuromorphic behavior, underlying the ion migration in dielectric layer (Figure 11c). Consequently, the EPSC value also gradually increased under the repetitive light spike (Figure 11d). Moreover, to realize the biomimetic sensorimotor system with a wireless optical communication method, the letter of the English alphabet was represented through the reactivity with the International Morse Coded light-spikes. Artificial sensorimotor synapses can identify international Morse codes by providing a unique EPSC pattern corresponding to each alphabetic letter represented by a pulse pattern of light spikes (Figure 11e). To verify the realization of human-machine interface using wireless optical

communication, a polymer actuator was connected to the synaptic transistor. As the number of light spikes increases, the EPSC gradually increases, indicating the strengthened synaptic connection. The accumulated EPSC with long-term potentiation characteristic continuously operates the actuator and increases the degree of fiber shrinkage (Figure 11f). This result denotes that the organic optoelectronic sensorimotor successfully suggests the neurosystem methodology for the biological neurobotic and soft electronics with wireless optical communication.

6. Conclusion

Overall, we reviewed state-of-the-art transistor-based optoelectronic synapses and their advanced applications for next-generation artificial intelligent system including neuromorphic in-memory computing, artificial sensory perception, and humanoid robotics. Compared with conventional electrical synapses

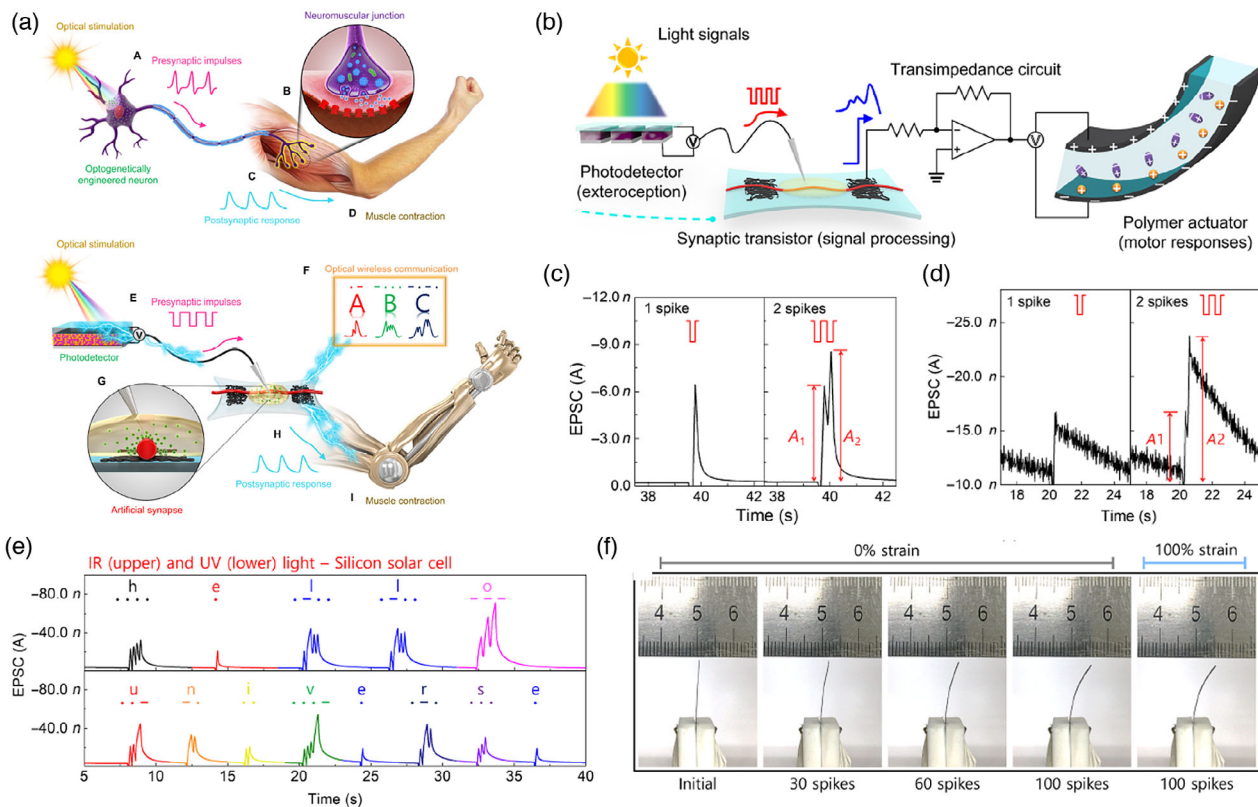


Figure 11. Optoelectronic synapse for a bioinspired sensorimotor system. a) schematic illustration of bioinspired neuromuscular electronic system. b) The artificial sensorimotor synapse consisting of photodetector, synaptic transistor, and polymer actuator, c) EPSC triggered by electrical spike, d) EPSC triggered by light spike, e) the EPSC triggered from optical Morse code of “HELLO UNIVERSE,” f) the contraction movement of artificial muscle according to the number of optical spikes. a–f) Reproduced with permission.^[106] Copyright 2018, AAAS.

using electrical spikes, optoelectronic synapses driven in optical spikes have distinctive advantages such as high processing speed, low power consumption, and mutual interference resistance, which can improve neuromorphic computing speed and suppress power consumption. To date, four types of transistor-based optoelectronic synapses have been proposed, including heterostructure channel, FG, amorphous oxide semiconductor, and integrated circuit types. These optoelectronic synapses can well mimic photosynaptic plasticity in optical spiking conditions, and can perform essential synaptic function including EPSC, IPSC, STM, LTM, and PPF. The driving mechanism and intrinsic advantageous of individual optoelectronic synapses were comprehensively discussed for photon-neuromorphic computing. Furthermore, the hardware implementation of advanced vision perception systems and humanoid robotics has been recently in the spotlight with the development of optoelectronic synapses showing excellent optical response.

However, there are still various challenging issues to implement optoelectronic synapse-based artificial intelligent system for photo-neuromorphic computing, artificial sensory perception, and humanoid robotics. Most surveys have been still conducted in single-device level, only mimicking fundamental synaptic plasticity and related functions. The future transistor-based optoelectronic synapses should be integrated in the form of array to achieve system-level neuromorphic computing, which will provide next-level problems including complex processing,

uniformity, and reliability issues. Also, the optical sources and wave guides for providing and transmitting massive optical inputs in system-level photoneuromorphic chip should be appropriately designed and integrated with optoelectronic synapse array. Meanwhile, optoelectronic synapse which can achieve bipolar photosynaptic dynamics in optical means should be developed. Although both positive (e.g., EPSC) and negative (e.g., IPSC) synaptic plasticities should be inevitably required for achieve photoneuromorphic computing, most optoelectronic synapse seldom trigger negative photoresponse. Most optoelectronic synapse achieve IPSC functions using electrical means, not optical input. Furthermore, the optoelectronic synapses with additional external sensory elements (touch, sound, gas, and tastes) and excellent mechanical flexibility should be developed to realize human-like integrated sensory platform and intelligent soft robotics.

Acknowledgements

This research was partially supported by the National Research Foundation of Korea (NRF) grant funded by the Korea government (MSIP) (Nos. NRF-2019R1A2C2002447 and NRF-2018R1D1A1B07050722), and the Engineering Research Center of Excellence (ERC) Program supported by National Research Foundation (NRF), Korean Ministry of Science & ICT (MSIT) (No. NRF-2017R1A5A1014708).

Conflict of Interest

The authors declare no conflict of interest.

Keywords

artificial sensory systems, neuromorphic computing, optoelectronic synapses, photo-synaptic plasticity, thin-film transistors

Received: July 16, 2020

Revised: October 9, 2020

Published online: February 5, 2021

- [1] P. A. Merolla, J. V. Arthur, R. Alvarez-Icaza, A. S. Cassidy, J. Sawada, F. Akopyan, B. L. Jackson, N. Imam, C. Guo, Y. Nakamura, B. Brezzo, I. Vo, S. K. Esser, R. Appuswamy, B. Taba, A. Amir, M. D. Flickner, W. P. Risk, R. Manohar, D. S. Modha, *Science* **2014**, 345, 668.
- [2] M. A. Zidan, J. P. Strachan, W. D. Lu, *Nat. Electron.* **2018**, 1, 22.
- [3] Y. Lee, T. W. Lee, *Acc. Chem. Res.* **2019**, 52, 964.
- [4] J. J. Harris, R. Jolivet, D. Attwell, *Neuron* **2012**, 75, 762.
- [5] L. F. Abbott, W. G. Regehr, *Nature* **2004**, 431, 796.
- [6] J. Tang, F. Yuan, X. Shen, Z. Wang, M. Rao, Y. He, Y. Sun, X. Li, W. Zhang, Y. Li, B. Gao, H. Qian, G. Bi, S. Song, J. J. Yang, H. Wu, *Adv. Mater.* **2019**, 31, 1902761.
- [7] H. E. Lee, J. H. Park, T. J. Kim, D. Im, J. H. Shin, D. H. Kim, B. Mohammad, I.-S. Kang, K. J. Lee, *Adv. Funct. Mater.* **2018**, 28, 1801690.
- [8] B. Sun, G. Zhou, T. Guo, Y. N. Zhou, Y. A. Wu, *Nano Energy* **2020**, 75, 104938.
- [9] C. Wan, P. Cai, M. Wang, Y. Qian, W. Huang, X. Chen, *Adv. Mater.* **2019**, 32, 1902434.
- [10] Y. H. Jung, B. Park, J. U. Kim, T. Kim, *Adv. Mater.* **2019**, 31, 1803637.
- [11] X. Ji, X. Zhao, M. C. Tan, R. Zhao, *Adv. Intell. Syst.* **2020**, 2, 1900118.
- [12] J. Yu, X. Yang, Q. Sun, *Adv. Intell. Syst.* **2020**, 2, 1900175.
- [13] H.-L. Park, Y. Lee, N. Kim, D.-G. Seo, G.-T. Go, T.-W. Lee, *Adv. Mater.* **2019**, 32, 1903558.
- [14] C. Wan, K. Xiao, A. Angelin, M. Antonietti, X. Chen, *Adv. Intell. Syst.* **2019**, 1, 1900073.
- [15] K. Xiao, C. Wan, L. Jiang, X. Chen, M. Antonietti, *Adv. Mater.* **2020**, 32, 2000218.
- [16] Y. Burgt, A. Melianas, S. T. Keene, G. Malliaras, A. Salleo, *Nat. Electron.* **2018**, 1, 386.
- [17] J.-Y. Mao, L. Zhou, X. Zhu, Y. Zhou, S.-T. Han, *Adv. Opt. Mater.* **2019**, 7, 1900766.
- [18] J. Zhang, S. Dai, Y. Zhao, J. Zhang, J. Huang, *Adv. Intell. Syst.* **2020**, 2, 1900136.
- [19] X. Zhuge, J. Wang, F. Zhuge, *Phys. Status Solidi RRL* **2019**, 13, 1900082.
- [20] Y. C. Shen, N. C. Harris, S. Skirlo, M. Prabhu, T. Baehr-Jones, M. Hochberg, X. Sun, S. J. Zhao, H. Larochelle, D. Englund, M. Soljacic, *Nat. Photonics* **2017**, 11, 441.
- [21] J. Feldmann, N. Youngblood, C. D. Wright, H. Bhaskaran, W. H. P. Pernice, *Nature* **2019**, 569, 208.
- [22] Z. Cheng, C. Rios, W. H. P. Pernice, C. D. Wright, H. Bhaskaran, *Sci. Adv.* **2017**, 3, e1700160.
- [23] D. Berco, D. S. Ang, *Adv. Intell. Syst.* **2019**, 1, 1900003.
- [24] J. J. Yang, D. B. Strukov, D. R. Stewart, *Nat. Nanotechnol.* **2013**, 8, 13.
- [25] D. S. Jeong, C. S. Hwang, *Adv. Mater.* **2018**, 30, 1704729.
- [26] V. K. Sangwan, M. C. Hersam, *Nat. Nanotechnol.* **2020**, 15, 517.
- [27] D. Ielmini, G. Pedretti, *Adv. Intell. Syst.* **2020**, 2, 2000040.
- [28] X.-B. Li, N.-K. Chen, X.-P. Wang, H.-B. Sun, *Adv. Funct. Mater.* **2018**, 28, 1803380.
- [29] Q. Xia, J. J. Yang, *Nat. Mater.* **2019**, 18, 309.
- [30] J. Wang, F. Zhuge, *Adv. Mater. Technol.* **2019**, 4, 1800544.
- [31] J. Lee, W. D. Lu, *Adv. Mater.* **2018**, 30, 1702770.
- [32] S. Dai, Y. Zhao, Y. Wang, J. Zhang, L. Fang, S. Jin, Y. Shao, J. Huang, *Adv. Funct. Mater.* **2019**, 29, 1903700.
- [33] B. Yan, B. Li, X. Qiao, C.-X. Xue, M.-F. Chang, Y. Chen, H. Li, *Adv. Intell. Syst.* **2019**, 1, 1900068.
- [34] Y. Ni, Y. Wang, W. Xu, *Small* **2020**, 1905332, <https://doi.org/10.1002/smll.201905332>.
- [35] H. Han, H. Yu, H. Wei, J. Gong, W. Xu, *Small* **2019**, 15, 1900695.
- [36] H. Ling, D. A. Koutsouras, S. Kazemzadeh, Y. Burgt, F. Yan, P. Gkoupidenis, *Appl. Phys. Rev.* **2020**, 7, 011307.
- [37] F. O. Schmitt, P. Dev, B. H. Smith, *Science* **1976**, 193, 1140.
- [38] A. Polsky, B. W. Mel, J. Schiller, *Nat. Neurosci.* **2004**, 7, 621.
- [39] A. E. Pereda, *Nat. Rev. Neurosci.* **2014**, 15, 250.
- [40] N. Spruston, Y. Schiller, G. Stuart, B. Sakmann, *Science* **1995**, 268, 297.
- [41] R. S. Zucker, W. G. Regehr, *Annu. Rev. Physiol.* **2002**, 64, 355.
- [42] L. F. Abbott, S. B. Nelson, *Nat. Neurosci.* **2000**, 3, 1178.
- [43] T. Ohno, T. Hasegawa, T. Tsuruoka, K. Terabe, J. K. Gimzewski, M. Aono, *Nat. Mater.* **2011**, 10, 591.
- [44] M.-K. Kim, J.-S. Lee, *ACS Nano* **2018**, 12, 1680.
- [45] T. Y. Wang, J.-L. Meng, Z.-Y. He, L. Chen, H. Zhu, Q.-Q. Sun, S.-J. Ding, D. W. Zhang, *Nanoscale Res. Lett.* **2019**, 14, 102.
- [46] Z. Wang, S. Joshi, S. E. Savel'ev, H. Jiang, R. Midya, P. Lin, M. Hu, N. Ge, J. P. Strachan, Z. Li, Q. Wu, M. Barnell, G.-L. Li, H. L. Xin, R. S. Williams, Q. Xia, J. J. Yang, *Nat. Mater.* **2017**, 16, 101.
- [47] D. Debanne, N. C. Guérineau, B. H. Gähwiler, S. M. Thompson, *J. Physiol.* **1996**, 491, 163.
- [48] K. Nomura, H. Ohta, K. Ueda, T. Kamiya, M. Hirano, H. Hosono, *Science* **2003**, 300, 1262.
- [49] Q. H. Wang, K. Kalantar-Zadeh, A. Kis, J. N. Coleman, M. S. Strano, *Nat. Nanotechnol.* **2012**, 7, 699.
- [50] D. K. Kim, Y. Lai, B. T. Diroll, C. B. Murray, C. R. Kagan, *Nat. Commun.* **2012**, 3, 1216.
- [51] H. Chen, H. Liu, Z. Zhang, K. Hu, X. Fang, *Adv. Mater.* **2016**, 28, 403.
- [52] N. Huo, G. Konstantatos, *Adv. Mater.* **2018**, 30, 1801164.
- [53] F. Teng, K. Hu, W. Ouyang, X. Fang, *Adv. Mater.* **2018**, 30, 1706262.
- [54] M. A. Haque, J.-L. Li, A. L. Abdelhady, M. I. Saidaminov, D. Baran, O. M. Bakr, S.-H. Wei, T. Wu, *Adv. Opt. Mater.* **2019**, 7, 1900865.
- [55] Y. Han, M. Fu, Z. Tang, X. Zheng, X. Ji, X. Wang, W. Lin, T. Yang, Q. Chen, *ACS Appl. Mater. Interfaces* **2017**, 9, 2867.
- [56] J.-Y. Wu, Y. T. Chun, S. Li, T. Zhang, J. Wang, P. K. Shrestha, D. Chu, *Adv. Mater.* **2018**, 30, 1705880.
- [57] L. Yin, W. Huang, R. Xiao, W. Peng, Y. Zhu, Y. Zhang, X. Pi, D. Yang, *Nano Lett.* **2020**, 20, 3378.
- [58] Z. Liu, S. Dai, Y. Wang, B. Yang, D. Hao, D. Liu, Y. Zhao, L. Fang, Q. Ou, S. Jin, J. Zhao, J. Huang, *Adv. Funct. Mater.* **2019**, 30, 1906335.
- [59] C. Qian, S. Oh, Y. Choi, J.-H. Kim, J. Sun, H. Huang, J. Yang, Y. Gao, J.-H. Park, J. H. Cho, *Nano Energy* **2019**, 66, 104095.
- [60] Y. Wang, Q. Wang, X. Zhan, F. Wang, M. Safdar, J. He, *Nanoscale* **2013**, 5, 8326.
- [61] W. Hu, J. Yang, *J. Mater. Chem. C* **2017**, 5, 12289.
- [62] C. Jia, Z. Lin, Y. Huang, X. Duan, *Chem. Rev.* **2019**, 119, 9074.
- [63] K. Chen, W. Gao, S. Emaminejad, D. Kiriya, H. Ota, H. Y. Y. Nyein, K. Takei, A. Javey, *Adv. Mater.* **2016**, 28, 4397.
- [64] G. W. Shim, W. Hong, J.-H. Cha, J. H. Park, K. J. Lee, S.-Y. Choi, *Adv. Mater.* **2020**, 32, 1907166.
- [65] H. Zhu, E.-S. Shin, A. Liu, D. Ji, Y. Xu, Y.-Y. Noh, *Adv. Funct. Mater.* **2019**, 30, 1904588.
- [66] C. Xie, C.-K. Liu, H.-L. Loi, F. Yan, *Adv. Funct. Mater.* **2020**, 30, 1903907.

- [67] W. Ouyang, F. Teng, J.-H. He, X. Fang, *Adv. Funct. Mater.* **2019**, *29*, 1807672.
- [68] J. Cheng, C. Wang, X. Zou, L. Liao, *Adv. Opt. Mater.* **2018**, 1800441.
- [69] S. W. Cho, S. M. Kwon, M. Lee, J.-W. Jo, J. S. Heo, Y.-H. Kim, H. K. Cho, S. K. Park, *Nano Energy* **2019**, *66*, 104097.
- [70] S. W. Cho, Y. B. Kim, S. H. Jung, S. K. Baek, J. S. Kim, M. Lee, H. K. Cho, Y.-H. Kim, *Adv. Opt. Mater.* **2018**, *6*, 1800196.
- [71] C.-C. Shih, W.-Y. Lee, W.-C. Chen, *Mater. Horizons* **2016**, *3*, 294.
- [72] Y. Wang, Z. Lv, J. Chen, Z. Wang, Y. Zhou, L. Zhou, X. Chen, S.-T. Han, *Adv. Mater.* **2018**, *30*, 1802883.
- [73] J. Sun, S. Oh, Y. Choi, S. Seo, M. J. Oh, M. Lee, W. B. Lee, P. J. Yoo, J. H. Cho, J.-H. Park, *Adv. Funct. Mater.* **2018**, *28*, 1804397.
- [74] H.-L. Park, H. Kim, D. Lim, H. Zhou, Y.-H. Kim, Y. Lee, S. Park, T.-W. Lee, *Adv. Mater.* **2020**, *32*, 1906899.
- [75] T.-Y. Wang, J.-L. Meng, Z.-Y. He, L. Chen, H. Zhu, Q.-Q. Sun, S.-J. Ding, P. Zhou, D. W. Zhang, *Adv. Sci.* **2020**, *7*, 1903480.
- [76] M. Lee, W. Lee, S. Choi, J. W. Jo, J. Kim, S. K. Park, Y. H. Kim, *Adv. Mater.* **2017**, *29*, 1700951.
- [77] Y. Chen, W. Qiu, X. Wang, W. Liu, J. Wang, G. Dai, Y. Yuan, Y. Gao, J. Sun, *Nano Energy* **2019**, *62*, 393.
- [78] Q. Wu, J. Wang, J. Cao, C. Lu, G. Yang, X. Shi, X. Chuai, Y. Gong, Y. Su, Y. Zhao, N. Lu, D. Geng, H. Wang, L. Li, M. Liu, *Adv. Electron. Mater.* **2018**, *4*, 1800556.
- [79] X. Yu, T. J. Marks, A. Facchetti, *Nat. Mater.* **2016**, *15*, 383.
- [80] T. Kamiya, H. Hosono, *NPG Asia Mater.* **2010**, *2*, 15.
- [81] A. Nathan, S. Lee, S. Jeon, J. Robertson, *J. Disp. Technol.* **2014**, *10*, 917.
- [82] A. Janotti, C. G. Walle, *Phys. Rev. B* **2007**, *76*, 165202.
- [83] J. E. Medvedeva, D. B. Buchholz, R. P. H. Chang, *Adv. Electron. Mater.* **2017**, *3*, 1700082.
- [84] K. Ide, K. Nomura, H. Hosono, T. Kamiya, *Phys. Status Solidi A* **2019**, *216*, 1800372.
- [85] S.-E. Ahn, I. Song, S. Jeon, Y. W. Jeon, Y. Kim, C. Kim, B. Ryu, J.-H. Lee, A. Nathan, S. Lee, G. T. Kim, U.-I. Chung, *Adv. Mater.* **2012**, *24*, 2631.
- [86] S. Jeon, S.-E. Ahn, I. Song, C. J. Kim, U.-I. Chung, E. Lee, I. Yoo, A. Nathan, S. Lee, K. Ghaffarzadeh, J. Robertson, K. Kim, *Nat. Mater.* **2012**, *11*, 301.
- [87] S. M. Kwon, S. W. Cho, M. Kim, J. S. Heo, Y.-H. Kim, S. K. Park, *Adv. Mater.* **2019**, *31*, 1906433.
- [88] H. Wang, Q. Zhao, Z. Ni, Q. Li, H. Liu, Y. Yang, L. Wang, Y. Ran, Y. Guo, W. Hu, Y. Liu, *Adv. Mater.* **2018**, *30*, 1803961.
- [89] S. Seo, S.-H. Jo, S. Kim, J. Shim, S. Oh, J.-H. Kim, K. Heo, J.-W. Choi, C. Choi, S. Oh, D. Kuzum, H.-S. P. Wong, J.-H. Park, *Nat. Commun.* **2018**, *9*, 5106.
- [90] H. Ling, D. A. Koutsouras, S. Kazemzadeh, Y. Burgt, F. Yan, P. Gkoupidenis, *Appl. Phys. Rev.* **2020**, *7*, 011307.
- [91] F. Yu, L. Q. Zhu, *Phys. Status Solidi RRL* **2019**, *13*, 1800674.
- [92] X. Bu, H. Xu, D. Shang, Y. Li, H. Lv, Q. Liu, *Adv. Intell. Syst.* **2020**, 2000156.
- [93] Y. Burgt, A. Melianas, S. T. Keene, G. Malliaras, A. Salleo, *Nat. Electron.* **2018**, *1*, 386.
- [94] S. H. Kim, K. Hong, W. Xie, K. H. Lee, S. Zhang, T. P. Lodge, C. D. Frisbie, *Adv. Mater.* **2013**, *25*, 1822.
- [95] G. Tarabella, F. M. Mohammadi, N. Coppede, F. Barbero, S. Iannotta, C. Santato, F. Ciccoira, *Chem. Sci.* **2013**, *4*, 1395.
- [96] Y.-G. Cho, C. Hwang, D. S. Cheong, Y.-S. Kim, H.-K. Song, *Adv. Mater.* **2019**, *31*, 1804909.
- [97] B. Nketia-Yawson, S.-J. Kang, G. D. Tabi, A. Perinot, M. Caironi, A. Facchetti, Y.-Y. Noh, *Adv. Mater.* **2017**, *29*, 1605685.
- [98] S. Seo, B.-S. Kang, J.-J. Lee, H.-J. Ryu, S. Kim, H. Kim, S. Oh, J. Shim, K. Heo, S. Oh, J.-H. Park, *Nat. Commun.* **2020**, *11*, 3936.
- [99] T. Ahmed, S. Kuriakose, S. Abbas, M. J. S. Spencer, M. A. Rahman, M. Tahir, Y. Lu, P. Sonar, V. Bansal, M. Bhaskaran, S. Sriram, S. Walia, *Adv. Funct. Mater.* **2019**, *29*, 1901991.
- [100] F. Yu, L. Q. Zhu, H. Xiao, W. T. Gao, Y. B. Guo, *Adv. Funct. Mater.* **2018**, *28*, 1804025.
- [101] Y. B. Guo, L. Q. Zhu, T. Y. Long, D. Y. Wan, Z. Y. Ren, *J. Mater. Chem. C* **2020**, *8*, 2780.
- [102] T. Ahmed, S. Kuriakose, E. L. H., Mayes, R. Ramanathan, V. Bansal, M. Bhaskaran, S. Sriram, S. Walia, *Small* **2019**, *15*, 1900966.
- [103] R. A. John, F. Liu, N. A. Chien, M. R. Kulkarni, C. Zhu, Q. Fu, A. Basu, Z. Liu, N. Mathews, *Adv. Mater.* **2018**, *30*, 1800220.
- [104] J. J. Yu, L. Y. Liang, L. X. Hu, H. X. Duan, W. H. Wu, H. L. Zhang, J. H. Gao, F. Zhuge, T. C. Chang, H. T. Cao, *Nano Energy* **2019**, *62*, 772.
- [105] E. Pastrana, *Nat. Methods* **2011**, *8*, 24.
- [106] Y. Lee, J. Y. Oh, W. Xu, O. Kim, T. R. Kim, J. Kang, Y. Kim, D. Son, J. B.-H. Tok, M. J. Park, Z. Bao, T.-W. Lee, *Sci. Adv.* **2018**, *4*, eaat7387.



Sung Woon Cho is an assistant professor of the Department of Printed Electronics Engineering, Suncheon National University, Suncheon, Korea. He received his Ph.D. in the School of Advanced Materials Science and Engineering from Sungkyunkwan University (SKKU), in 2018. His recent research interests are focused on metal-oxide thin-film transistors and their optoelectronic application for neuromorphic in-memory computing hardware, artificial sensory perception systems, and biomimetic robotics.



Sung Min Kwon received his M.S degree in the School of Electrical and Electronics Engineering at Chung-Ang University. He continued to be a Ph.D. degree student in the School of Electrical and Electronics Engineering at Chung-Ang University. His research interest focused on the display, advanced memory, and optoelectronic device based on metal-oxide, metal-chalcogenide, and QD materials.



Yong-Hoon Kim is an associate professor of the School of Advanced Materials Science and Engineering, Sungkyunkwan University, Suwon, Korea. He received his Ph.D. from Seoul National University, Seoul, Korea, in 2010. He worked at Korea Electronics Technology Institute as a managerial researcher in the Department of Flexible Display Research Center. At Sungkyunkwan University, his research focuses on developing flexible electronic devices including flexible displays, wearable sensors, and other innovative electronic devices. His current areas of research interest include textile-based wearable electronics, low-temperature solution processing of high-performance devices, and bioinspired neuromorphic devices.



Sung Kyu Park is the professor of School of Electrical and Electronics Engineering at Chung-Ang University, Seoul, Korea. He received his Ph.D degree from The Pennsylvania State University, University Park, PA in 2007. He was employed at Korea Electronics Technology Institute (KETI) and Eastman Kodak Company, Rochester, NY. Prof. Park's research focuses on exploratory electronic materials and devices. His current areas of research interest include quantum dots, organic, metal-oxide, chalcogenide materials and their applications such as electronic devices, fiber-based electronics, wearable sensors, display technologies, and neuromorphic systems.